Data reduction of 1ES 1426+428 And The outburst of BL Lacertae

Chang et al.(2024)

Reporter: Xin Chang (常鑫)
email: cx@mail.ynu.edu.cn
Yunnan University
SWIFAR
2024-10-15

1. Data processing steps
2. Data processing results
3. Data processing comparison
4. Current outburst of BL Lacertae

Data processing steps

- 1.Original Images: Firstly, it is necessary to obtain the target star's original image, background image, and flat-field image from observations.
- 2. Bias: the recorded CCD output image during a zero-second exposure when there is no signal input. This occurs because even when the CCD is not receiving photons, it still generates electrons as an inherent property of the CCD.
- 3. Flat: due to the fact that each pixel on the CCD does not have completely uniform sensitivity to photon response, there will be differences even in the response to a uniform light source. Therefore, before or after observing celestial objects, a uniform light source is also photographed as a comparison standard, which is called a flat-field.
- 4. Preprocessing: with the bias and flat images, initial preprocessing can be done on the original image to obtain a clean image. The principle of processing is as follows:

$$Target\ Image = \frac{Original\ Image - bias}{flat - bias}$$

Data processing steps

- 1.Image Alignment (SWarp): SWarp can resample multiple images with different World Coordinate Systems (WCS) onto a common WCS coordinate framework and stack them. If only one image is input and the WCS information of another image is used as the target coordinate framework for resampling, the alignment of the two images can be achieved. During the resampling process, SWarp calculates the corresponding pixel coordinates on the input image for each pixel position in the output image based on the WCS information. It then computes the pixel value at this pixel coordinate by interpolating the pixels near this position on the input image, and subsequently fills this value into the corresponding position on the output image.

- 2.Flux Calibration: Due to impacts such as instrumental effects, weather variations, or atmospheric changes (e.g., atmospheric refraction, turbulence, telescope gravitational distortion, etc.), the flux in each image can vary. Therefore, flux calibration is necessary.
- We select the image with the best quality and choose different standard stars. By subtracting the standard stars in this image from those in other images, we obtain the flux difference for each standard star. The flux of each standard star is then divided by its corresponding flux difference to obtain a calibration factor. The median of these calibration factors is taken, and each other image is multiplied by this median value to complete the flux calibration.

Data processing steps

Comparison of Flux Calibration for g-band on May 18, 2023

- Since the zero point has already undergone flux correction, the step of flux calibration was not performed. After adding the zero point, the results with and without flux calibration are identical.
- The above figure shows the light curve without adding the zero point after flux calibration, while the below figure shows the light curve with the zero point added but without flux calibration. The root mean square error between the two light curves is 0.001507642.

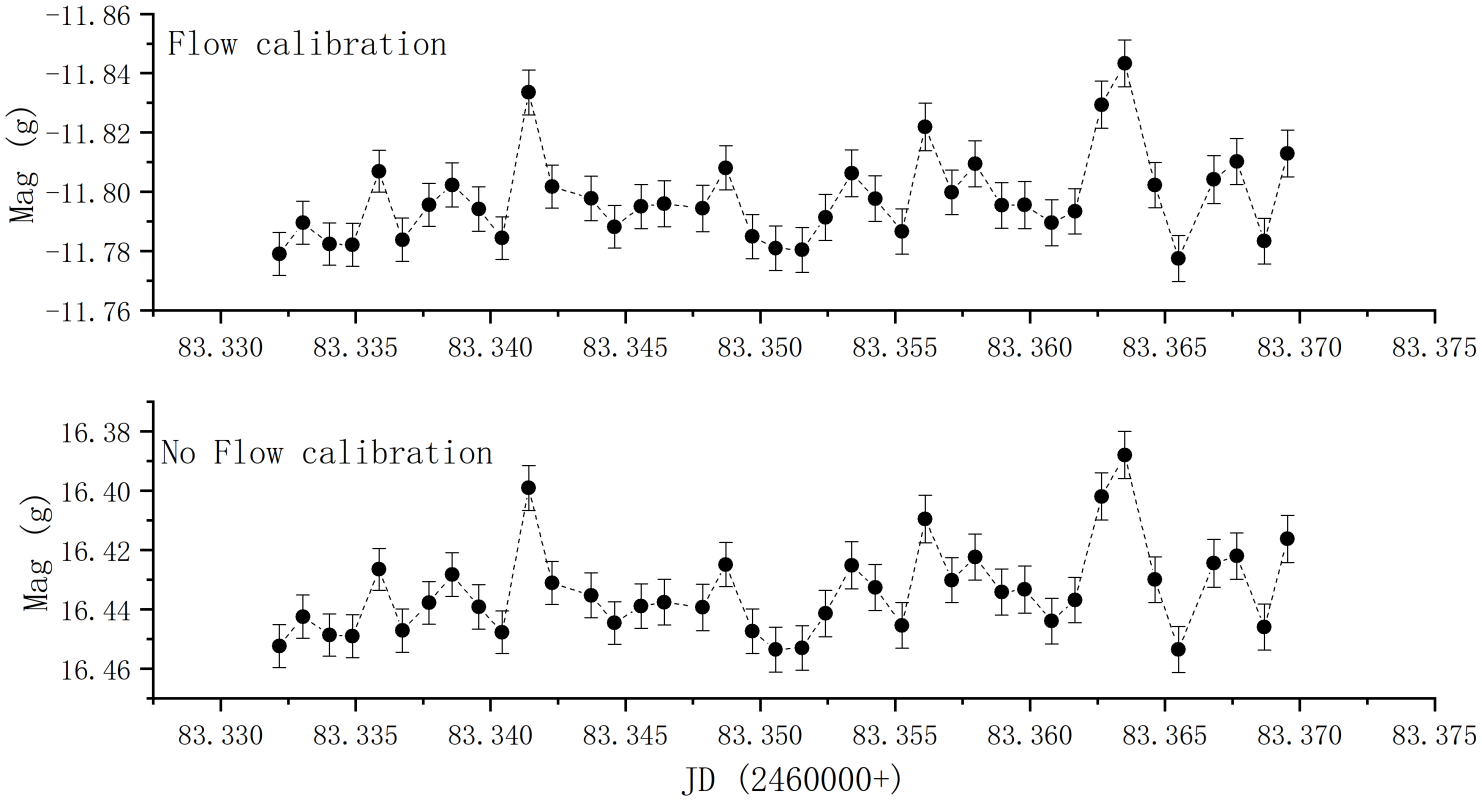

Data processing steps

- Image Subtraction: The purpose of image subtraction is to eliminate as much as possible the unchanged (or identical) parts in two images, such as point sources and extended sources with constant positions and brightness, thereby highlighting the varying parts, like newly emerging transient sources in scientific images. Because the target source AGN we observed exhibits minimal changes, the images processed by hotpants are relatively dark. Therefore, we did not use hotpants for image subtraction and proceeded directly with photometry.

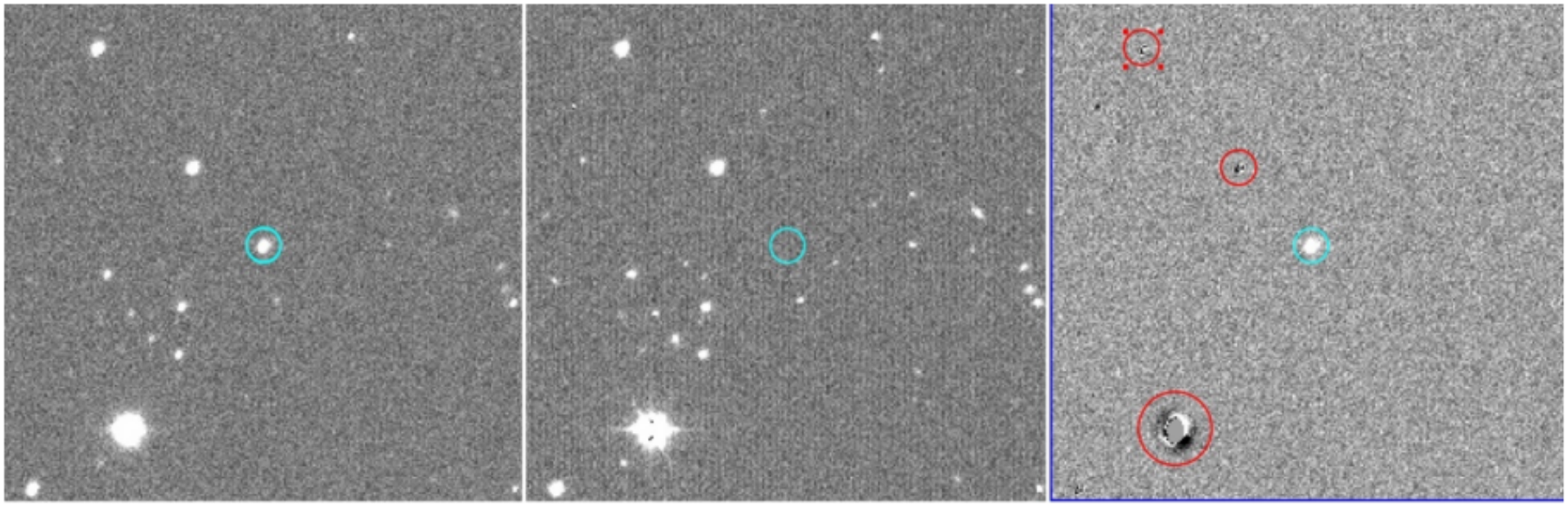

Data processing steps

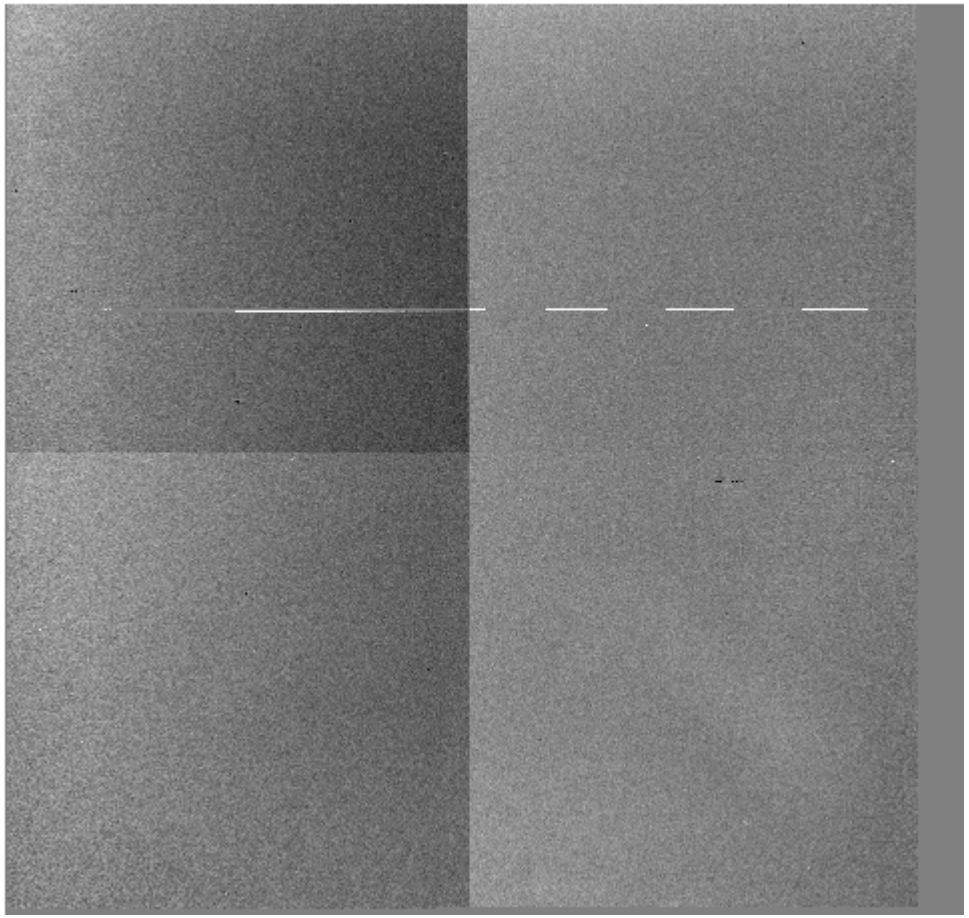

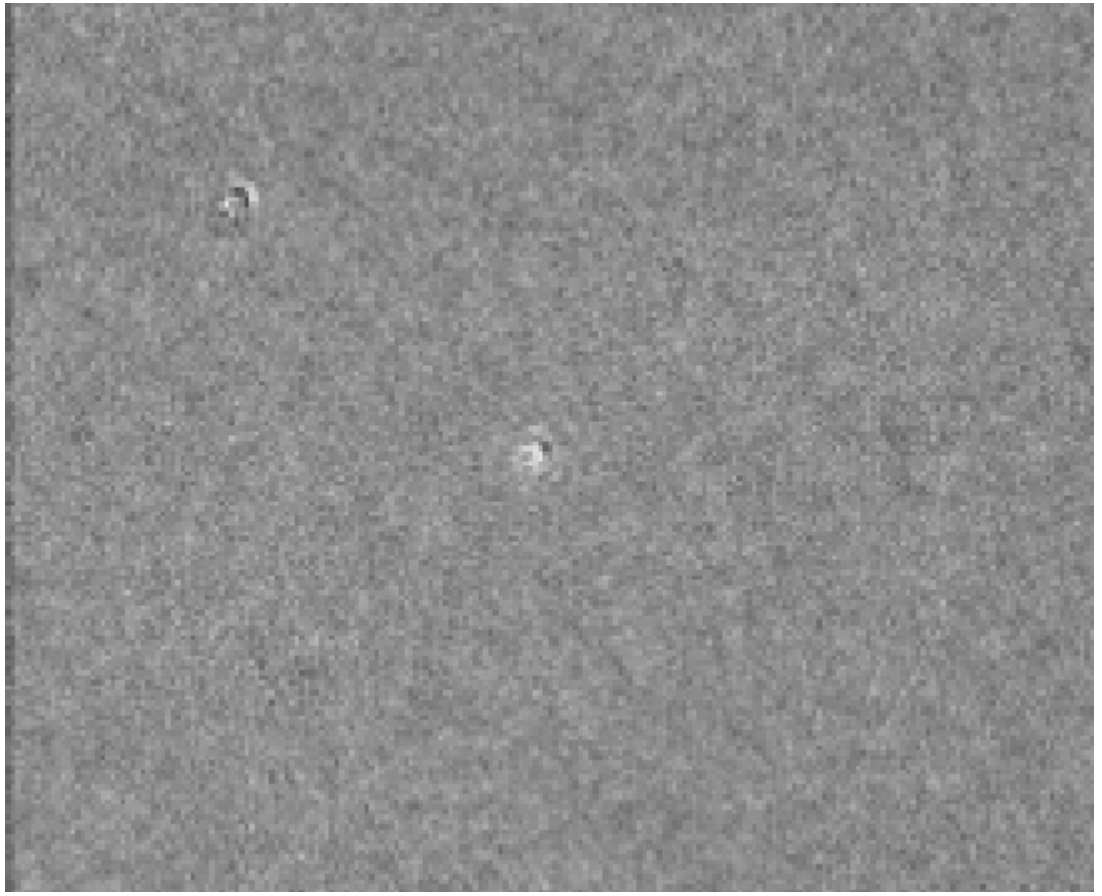

Data processing steps

- Aperture Photometry (Sextractor): Aperture photometry involves aligning a selected aperture size with the point source to be measured, counting the total number of photons within the aperture, and then subtracting the number of background photons to obtain the flux of the point source. Subsequently, the instrumental magnitude is calculated based on this flux.

$$Number\ of\ pixels\ in\ the\ target\ aperture = a_0,$$

$$Number\ of\ pixels\ in\ the\ sky\ backgroundregion = a_s,$$

$$Total\ sum\ of\ readingsin\ the\ target\ aperture = D_0,$$

$$Total\ sum\ of\ readings\ in\ the\ sky\ background\ region = D_s,$$

$$Number\ of\ photoelectrons\ corresponding\ to\ one\ reading = GAIN.$$

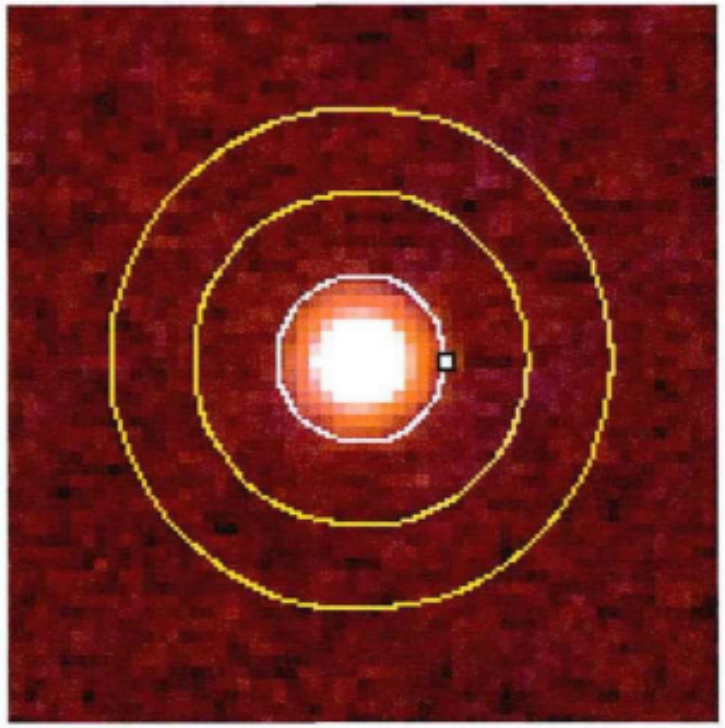

$$S_0 = \mathrm{GAIN} \cdot (D_0 - D_s \cdot (a_0/a_s))$$

$$M_{\mathrm{inst}} = -2.5\log_{10}(\mathrm{S})$$

Data processing steps

- **Zeropoint:**
- The AB magnitude system is a magnitude system based on flux density, with its zeropoint defined as the specific flux density of Vega in the V-band.

$$AB = -2.5 \log F_\nu - 48.60$$

$$m^{\mathrm{obs}} = -2.5 \log_{10} \left(\frac{\int_0^\infty F_\nu(\lambda) \times S^{\mathrm{obs}}(\lambda) \times \mathrm{d}\lambda}{\int_0^\infty S^{\mathrm{obs}}(\lambda) \times \mathrm{d}\lambda} \right) - 48.60$$

- Using the XP spectrum from Gaia and the transmission rate of our filter, perform a convolution to obtain the corresponding magnitude. By subtracting the observed instrumental magnitude from the obtained magnitude, the corresponding zeropoint can be determined.
- As for the first step of correcting the instrumental magnitude, it involves adjusting for the effects of exposure time and atmospheric absorption. Here, k' represents the atmospheric extinction coefficient, which can be derived through a least squares linear regression analysis by observing the same standard star at different times and under varying airmasses, or by observing different standard stars at (nearby) times and under different airmasses. X denotes the airmass, which can be retrieved from the information in the image header file.

$$m' = m_i + 2.5 \log_{10}(t_{\mathrm{exp}}) - k' X$$

1m6 reduction results

- Below are the light curves for each band and each day in the database;
- The final table presents the number of data points, mean square error, average Sextractor error, and nightly amplitude for each band and each day.

g band

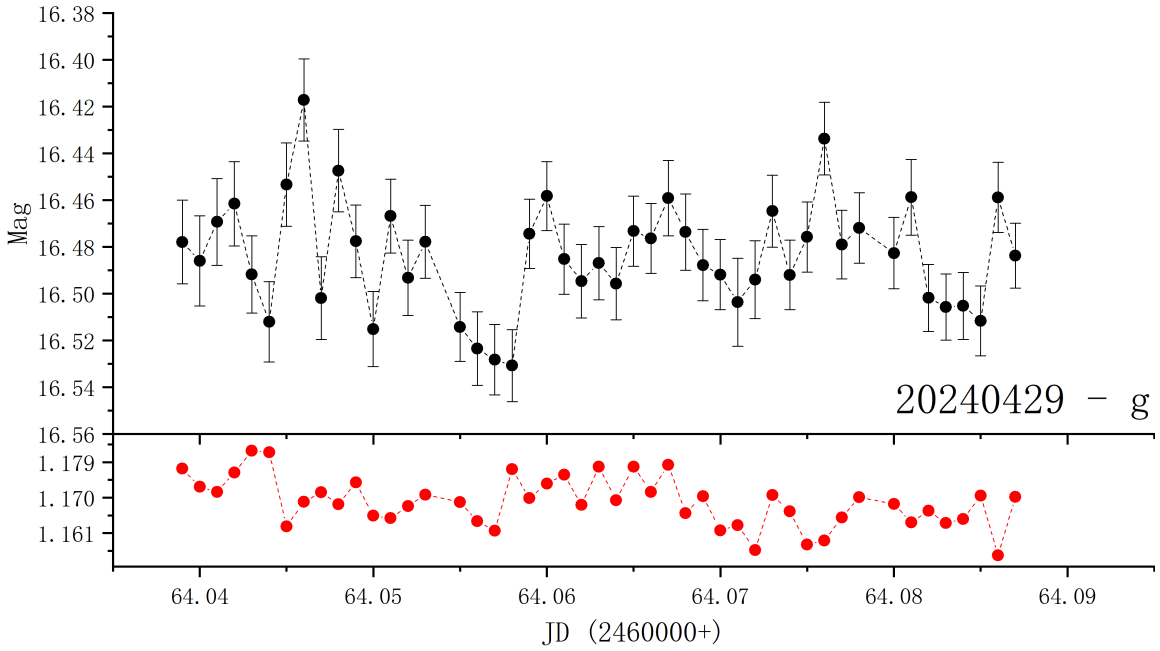
Mag
16.38
16.40
16.42
16.44
16.46
16.48
16.50
16.52
16.54
16.56
20240429 - g
1.179
1.170
1.161
64.04
64.05
64.06
64.07
64.08
64.09
JD (2460000+)

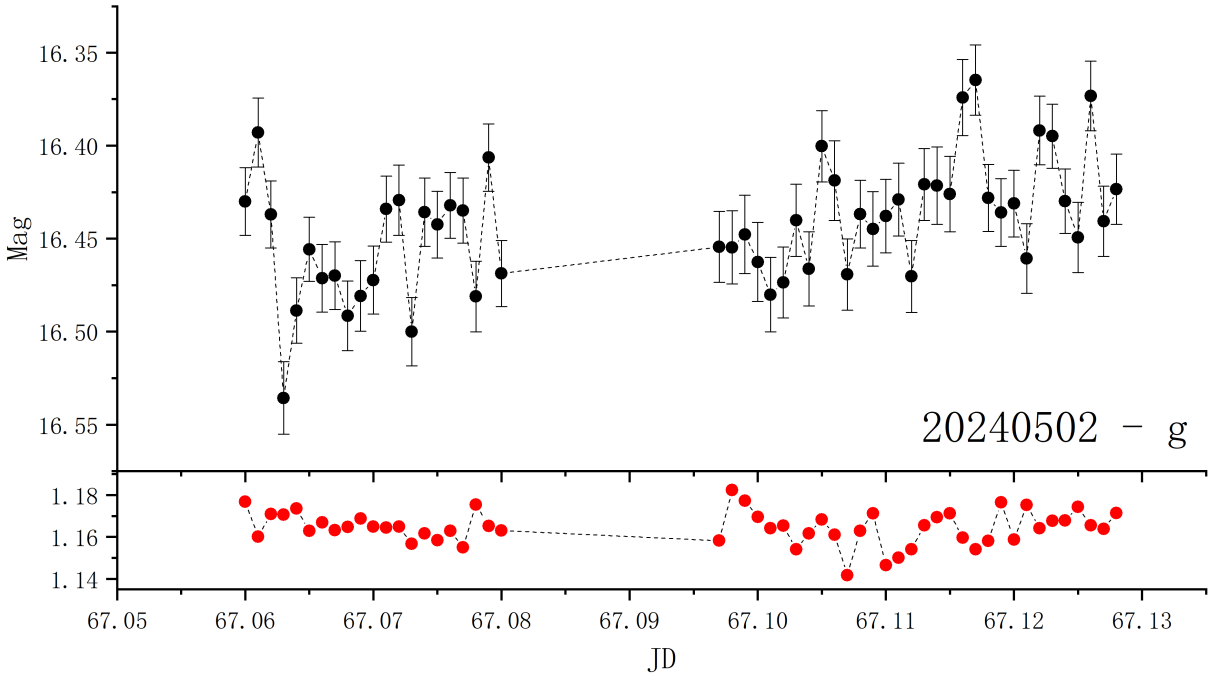
Mag
16.35
16.40
16.45
16.50
16.55
20240502 - g
1.18
1.16
1.14
67.05
67.06
67.07
67.08
67.09
67.10
67.11
67.12
67.13
JD

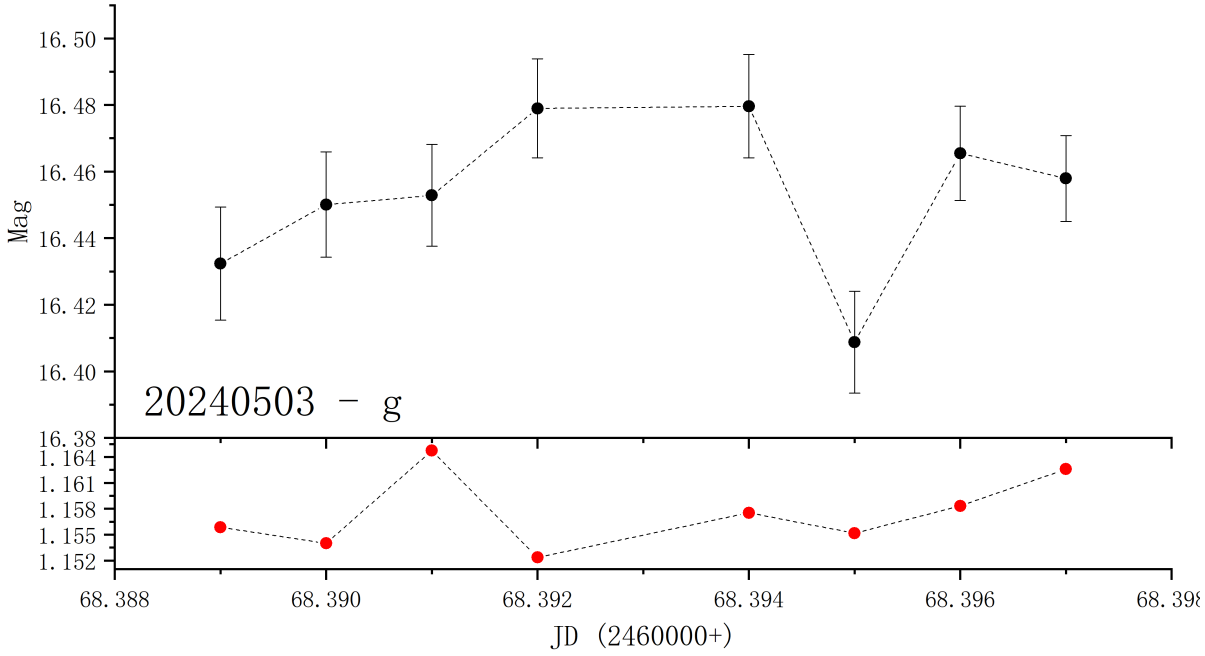
Mag
16.50
16.48
16.46
16.44
16.42
16.40
16.38
20240503 - g
1.164
1.161
1.158
1.155
1.152
68.388
68.390
68.392
68.394
68.396
68.398
JD (2460000+)

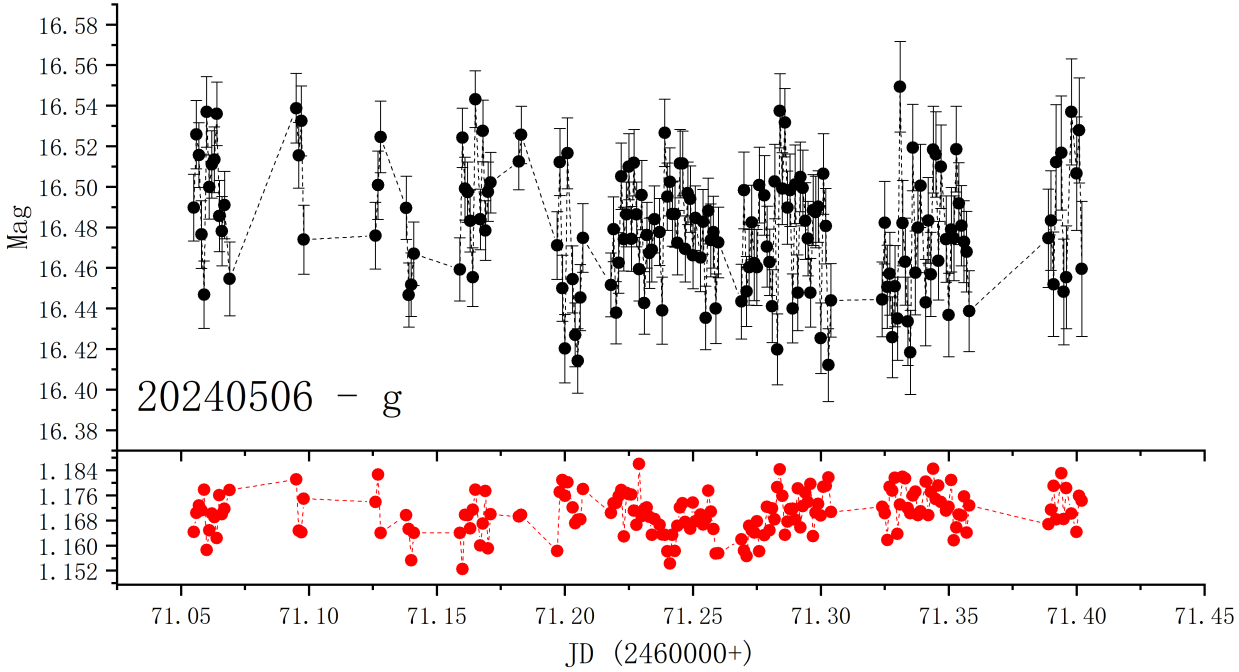
Mag
16.58
16.56
16.54
16.52
16.50
16.48
16.46
16.44
16.42
16.40
16.38
20240506 - g
1.184
1.176
1.168
1.160
1.152
71.05
71.10
71.15
71.20
71.25
71.30
71.35
71.40
71.45
JD (2460000+)

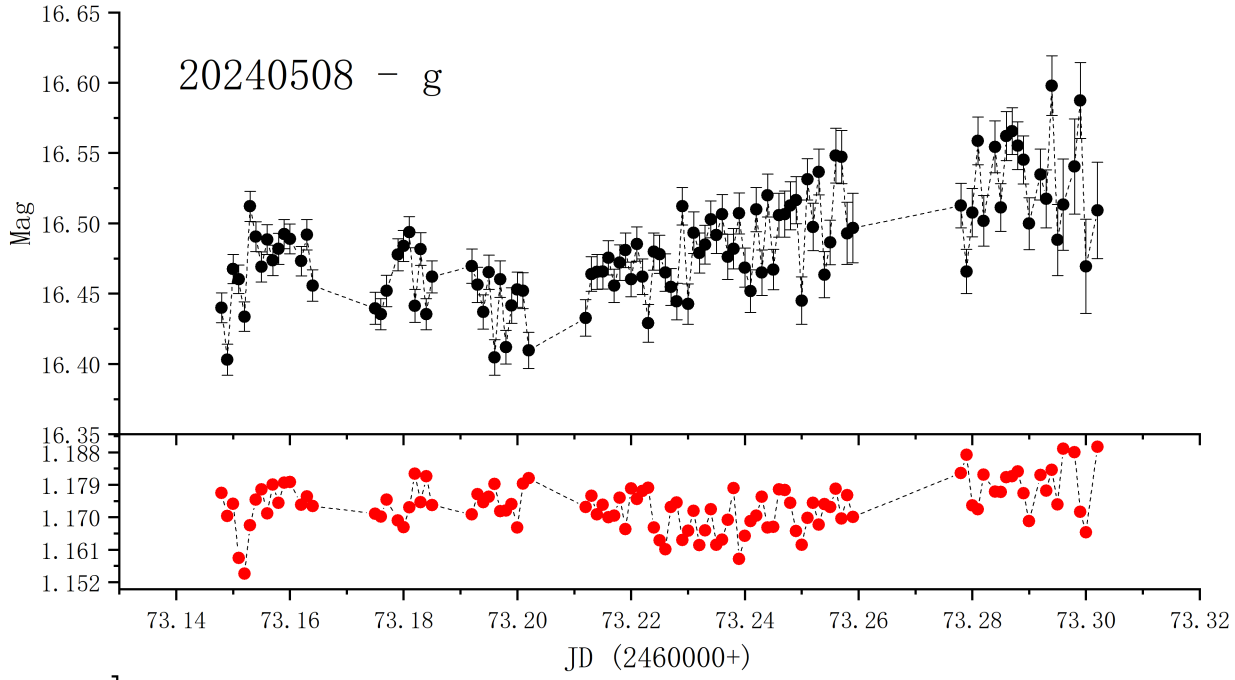
20240508 - g
Mag
16.65
16.60
16.55
16.50
16.45
16.40
16.35
1.188
1.179
1.170
1.161
1.152
73.14
73.16
73.18
73.20
73.22
73.24
73.26
73.28
73.30
73.32
JD (2460000+)

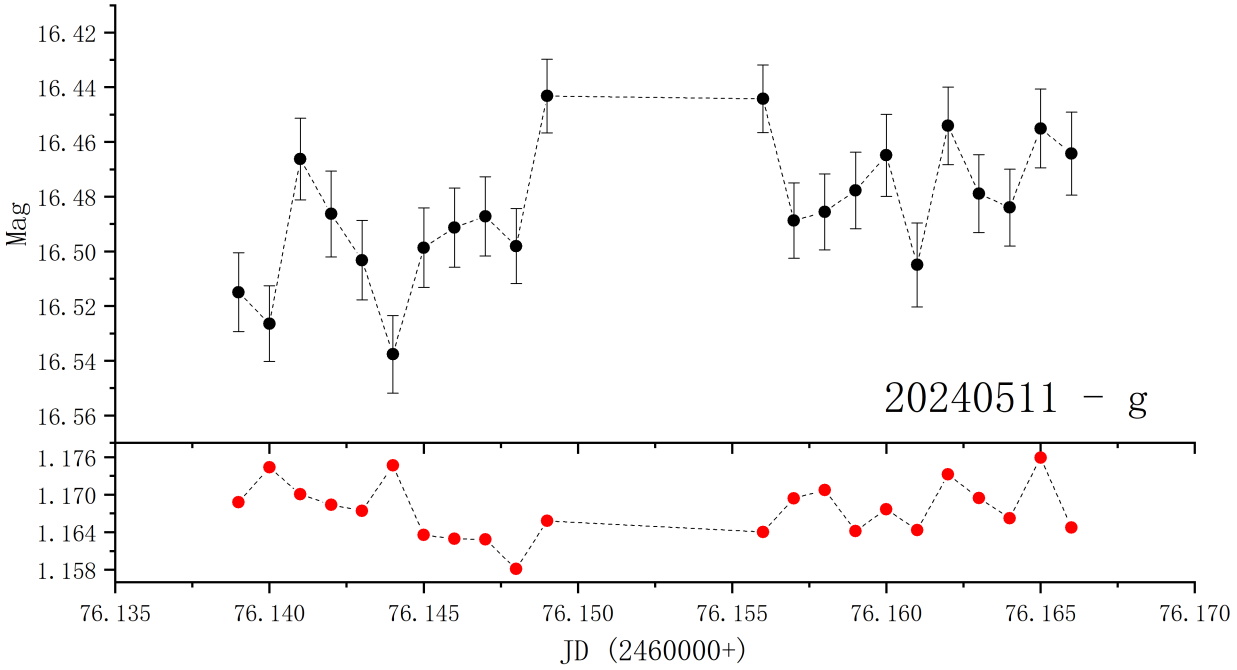
20240511 - g
Mag
16.42
16.44
16.46
16.48
16.50
16.52
16.54
16.56
1.176
1.170
1.164
1.158
76.135
76.140
76.145
76.150
76.155
76.160
76.165
76.170
JD (2460000+)

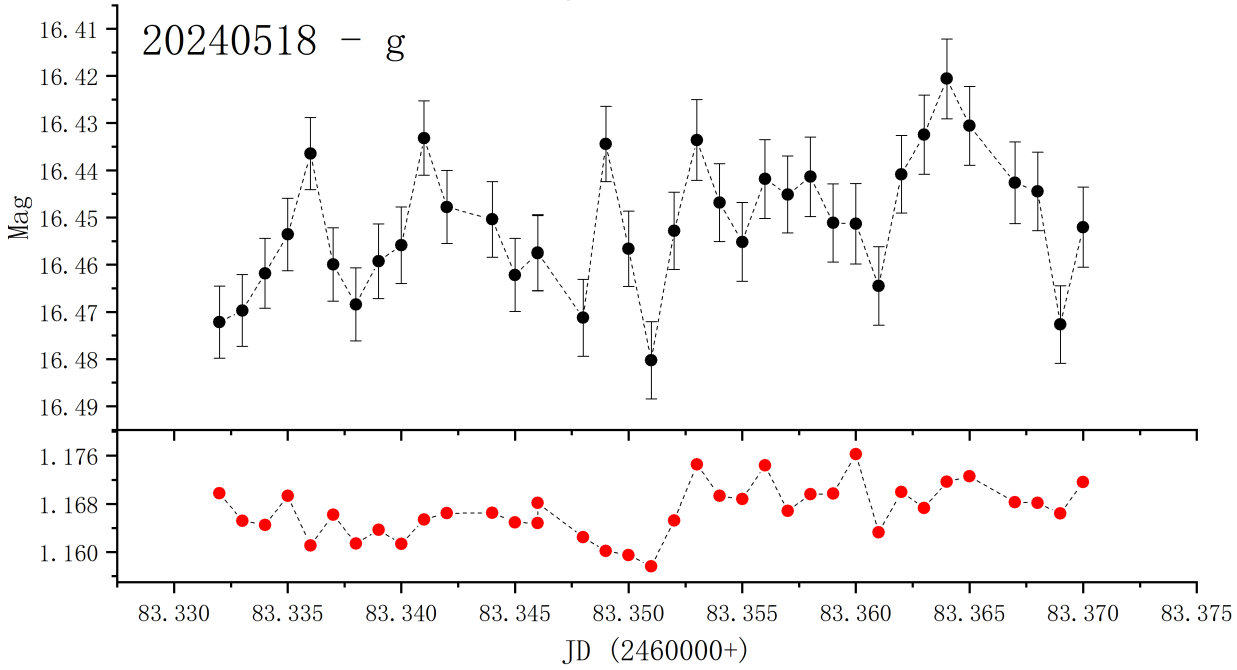
20240518 - g
Mag
16.41
16.42
16.43
16.44
16.45
16.46
16.47
16.48
16.49
1.176
1.168
1.160
83.330
83.335
83.340
83.345
83.350
83.355
83.360
83.365
83.370
83.375
JD (2460000+)

u band

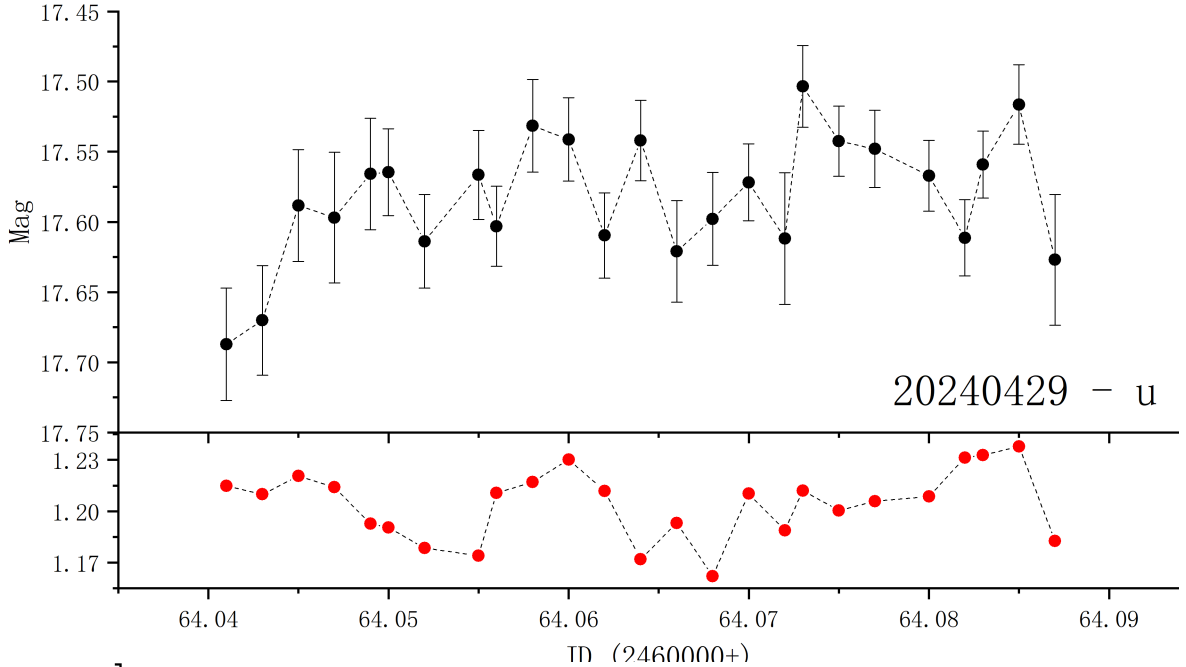
Mag
17.45
17.50
17.55
17.60
17.65
17.70
17.75
20240429 - u
1.23
1.20
1.17
64.04
64.05
64.06
64.07
64.08
64.09

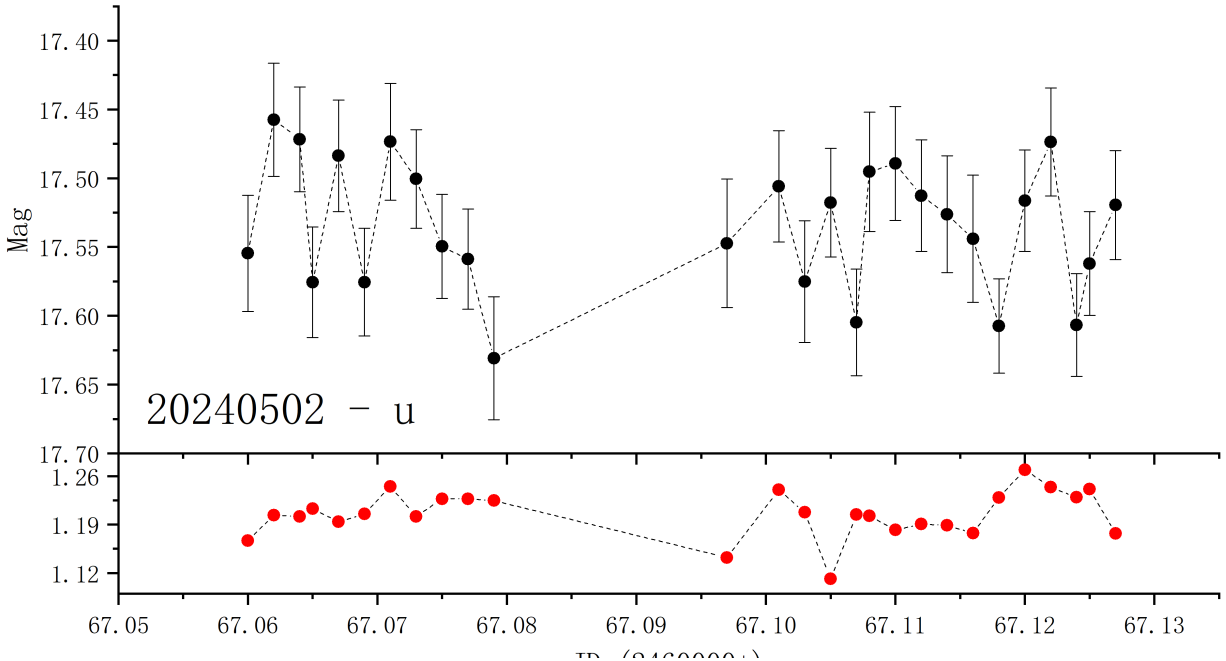
Mag
17.40
17.45
17.50
17.55
17.60
17.65
17.70
20240502 - u
1.26
1.19
1.12
67.05
67.06
67.07
67.08
67.09
67.10
67.11
67.12
67.13

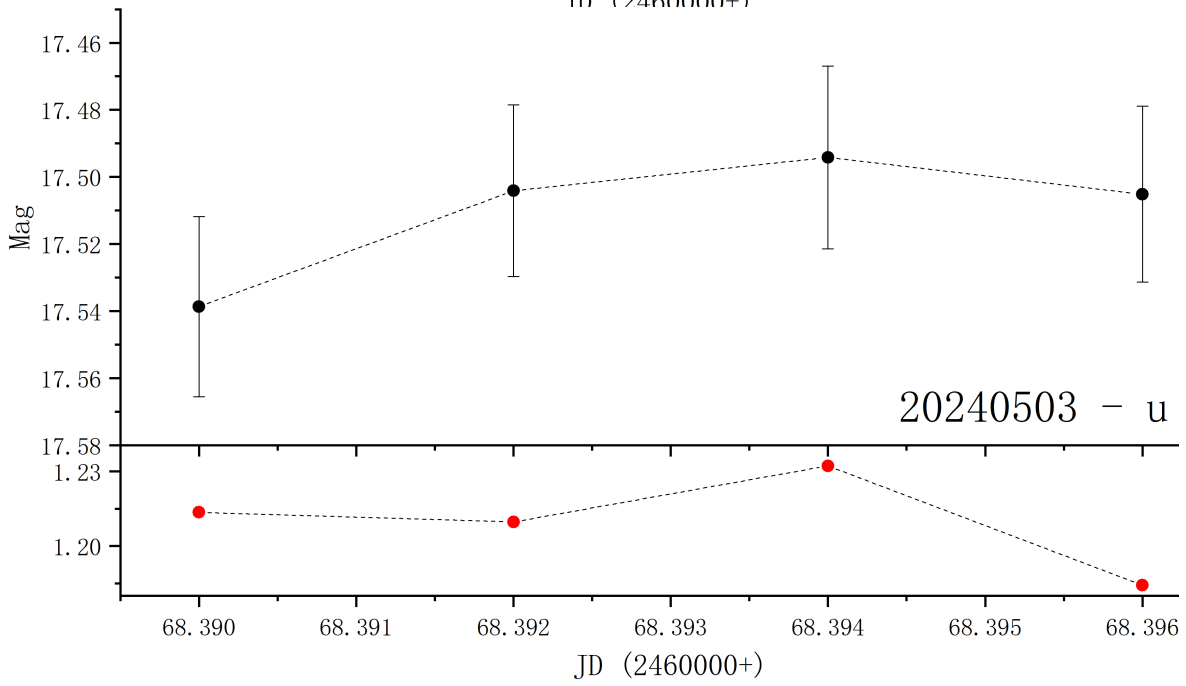
Mag
17.46
17.48
17.50
17.52
17.54
17.56
17.58
20240503 - u
1.23
1.20
68.390
68.391
68.392
68.393
68.394
68.395
68.396
JD (2460000+)

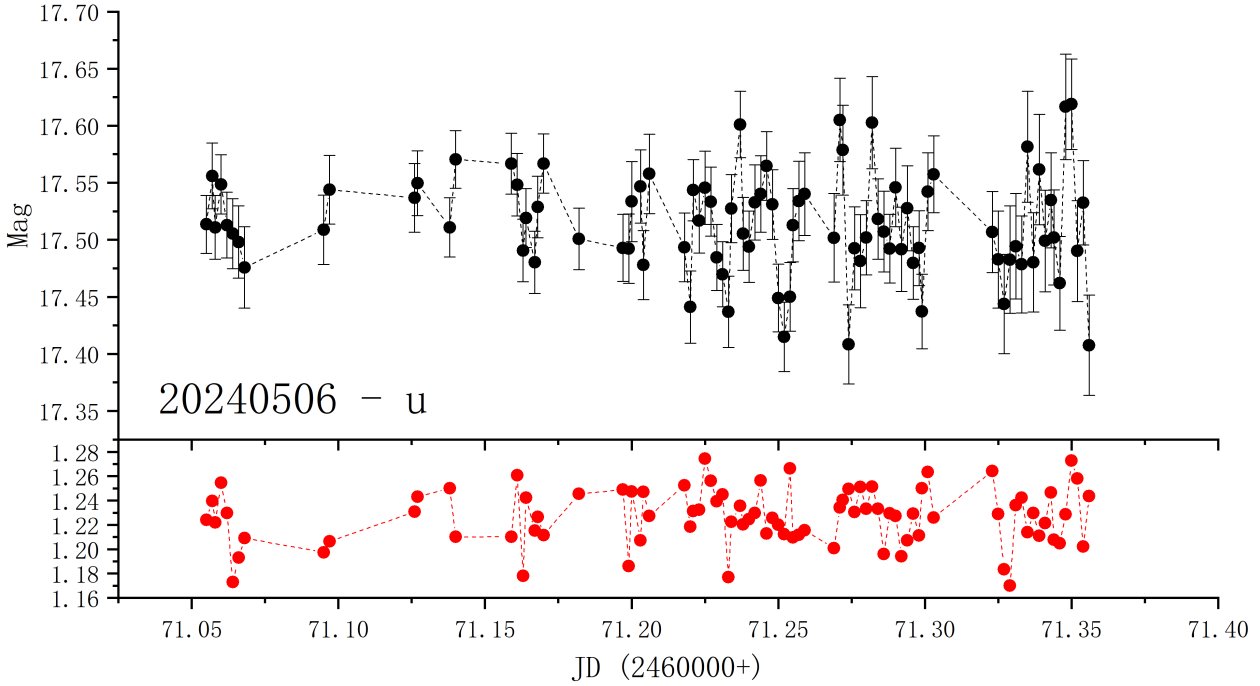
Mag
17.70
17.65
17.60
17.55
17.50
17.45
17.40
17.35
20240506 - u
1.28
1.26
1.24
1.22
1.20
1.18
1.16
71.05
71.10
71.15
71.20
71.25
71.30
71.35
71.40
JD (2460000+)

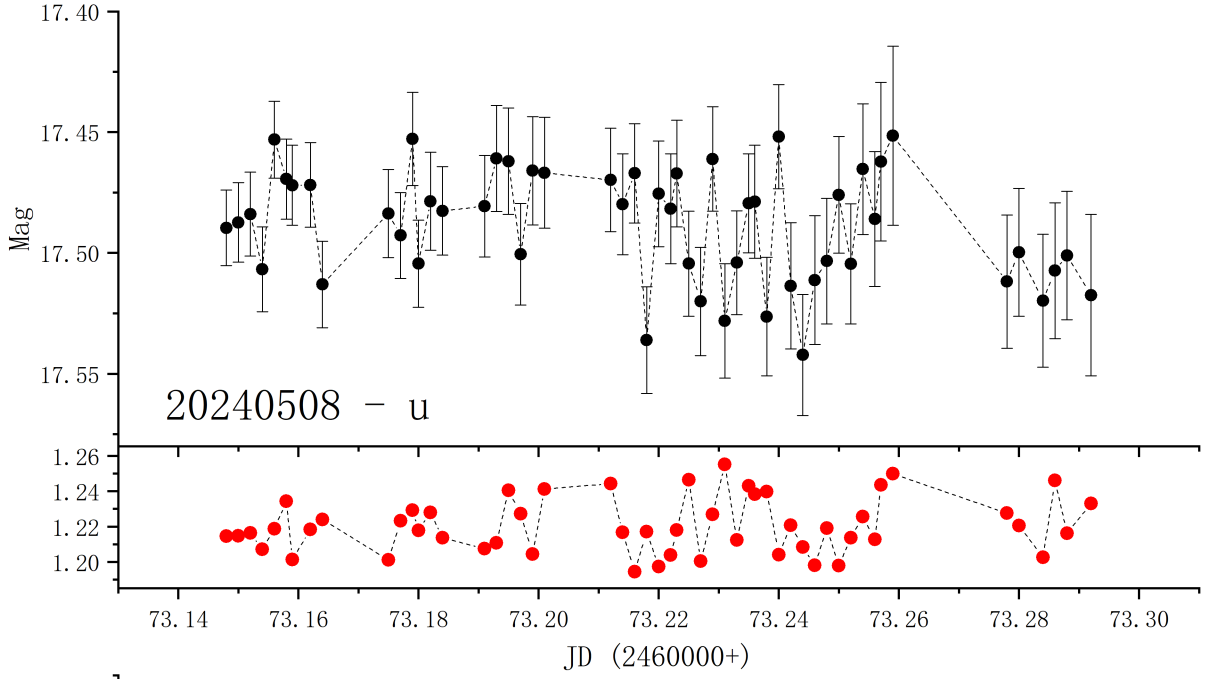
20240508 - u
Mag
17.40
17.45
17.50
17.55
1.26
1.24
1.22
1.20
73.14
73.16
73.18
73.20
73.22
73.24
73.26
73.28
73.30
JD (2460000+)

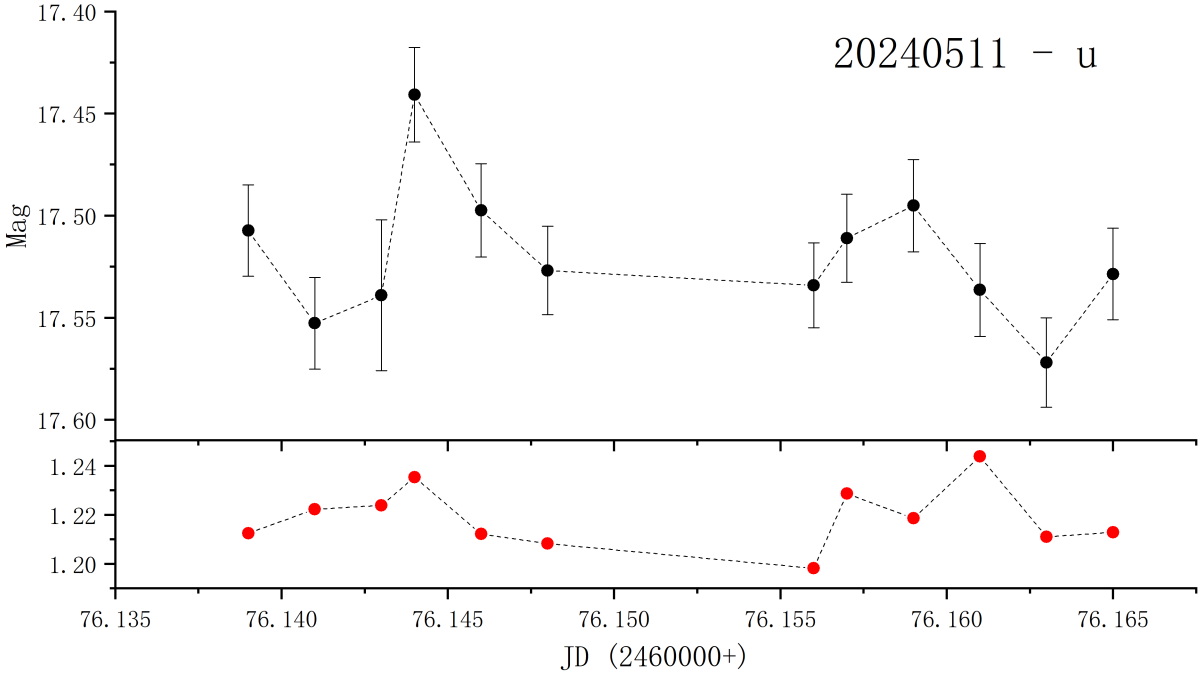
20240511 - u
Mag
17.40
17.45
17.50
17.55
17.60
1.24
1.22
1.20
76.135
76.140
76.145
76.150
76.155
76.160
76.165
JD (2460000+)

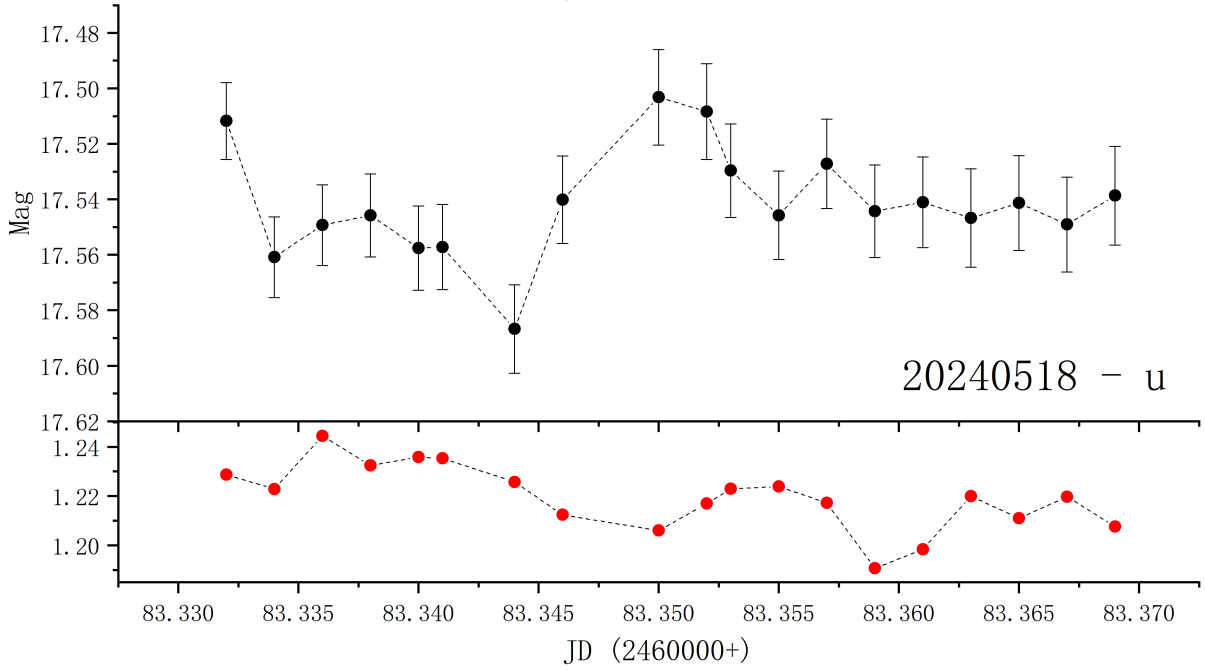
20240518 - u
Mag
17.48
17.50
17.52
17.54
17.56
17.58
17.60
17.62
1.24
1.22
1.20
83.330
83.335
83.340
83.345
83.350
83.355
83.360
83.365
83.370
JD (2460000+)

r band

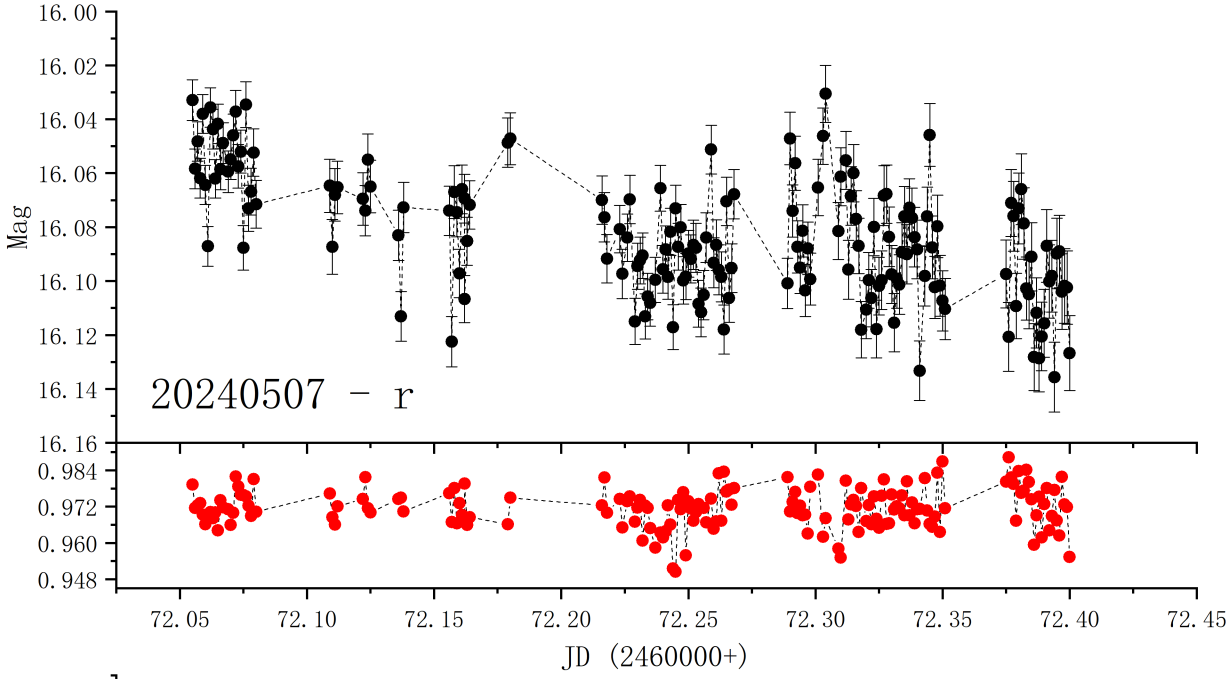
20240507 - r
Mag
JD (2460000+)

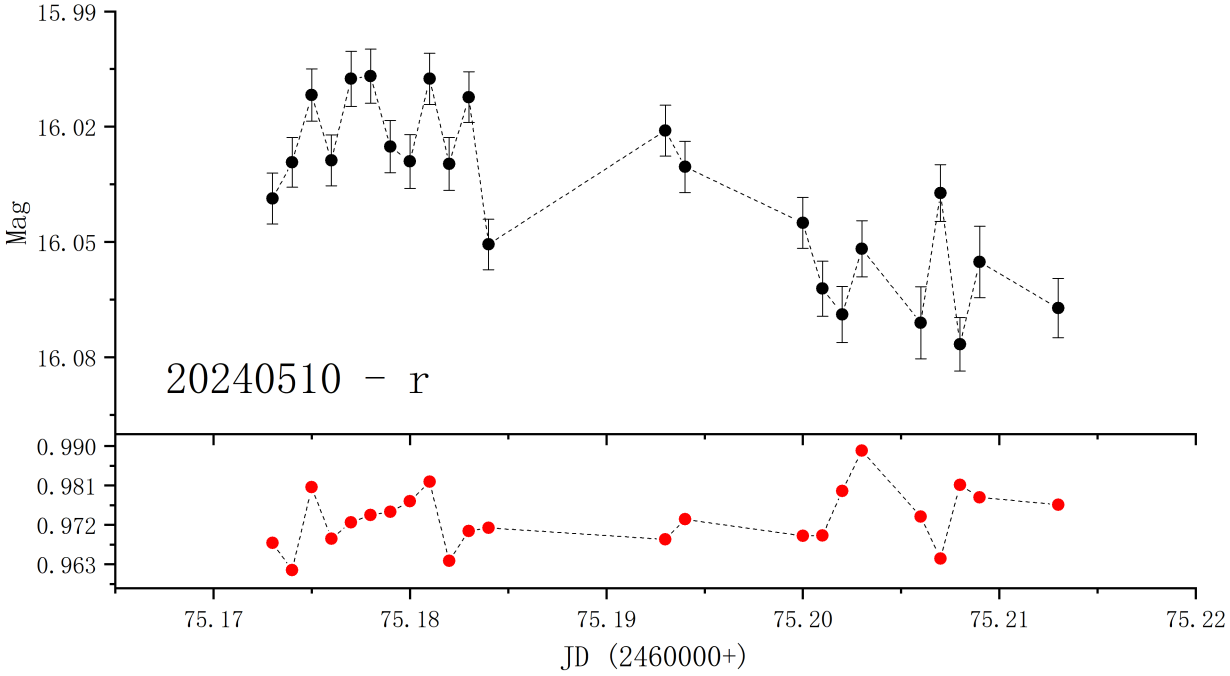
20240510 - r
Mag
JD (2460000+)

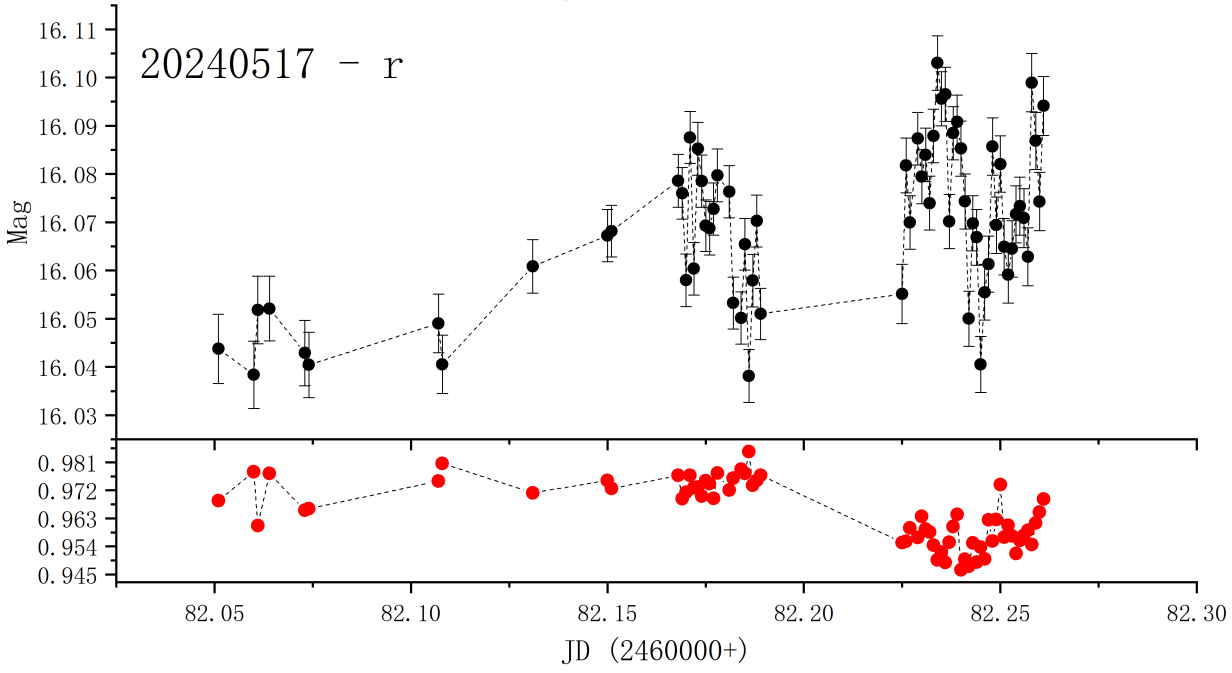
20240517 - r
Mag
JD (2460000+)

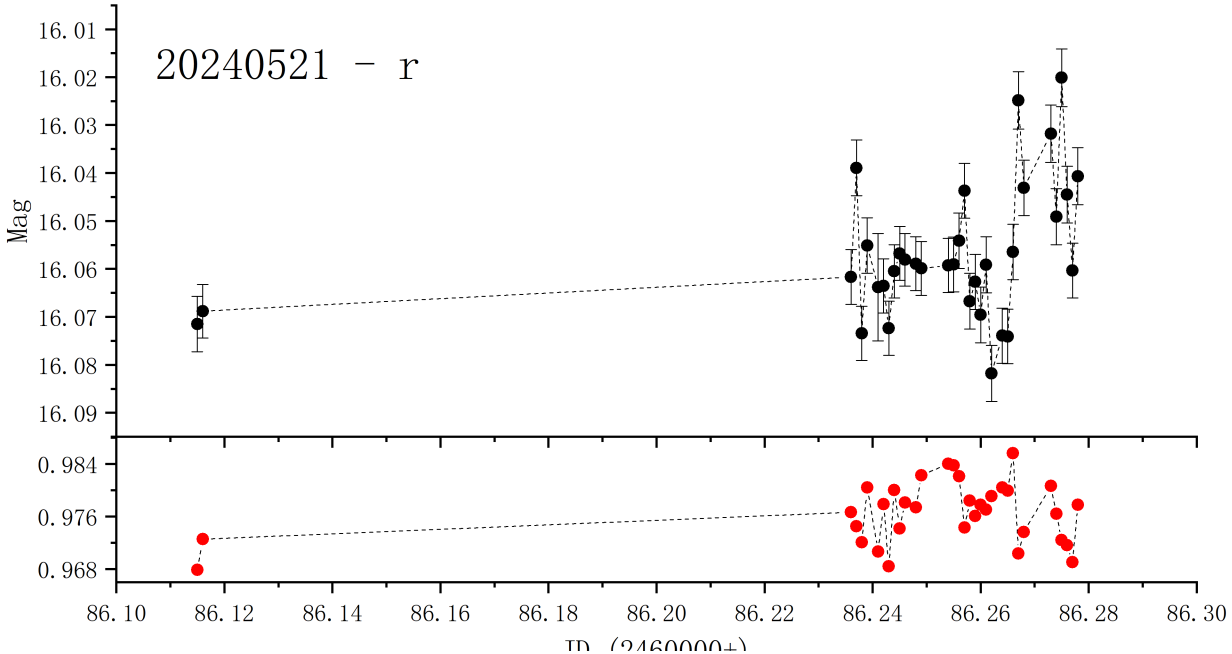
20240521 - r
Mag
16.01
16.02
16.03
16.04
16.05
16.06
16.07
16.08
16.09
0.984
0.976
0.968
86.10
86.12
86.14
86.16
86.18
86.20
86.22
86.24
86.26
86.28
86.30

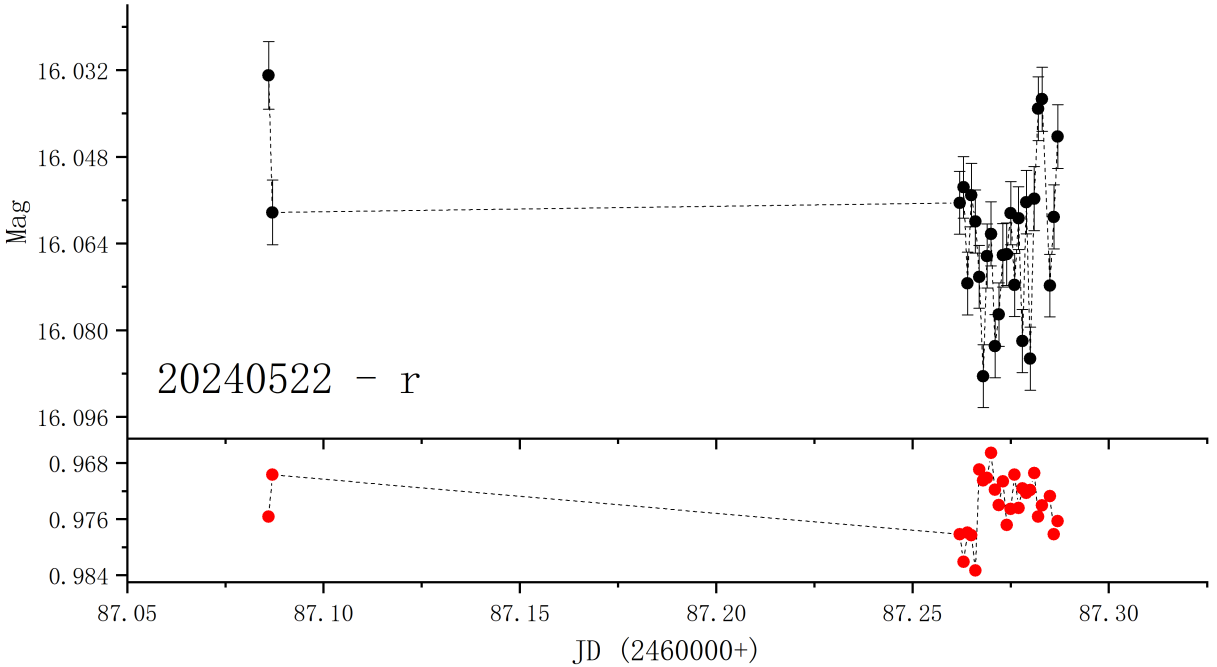
20240522 - r
Mag
16.032
16.048
16.064
16.080
16.096
0.968
0.976
0.984
87.05
87.10
87.15
87.20
87.25
87.30
JD (2460000+)

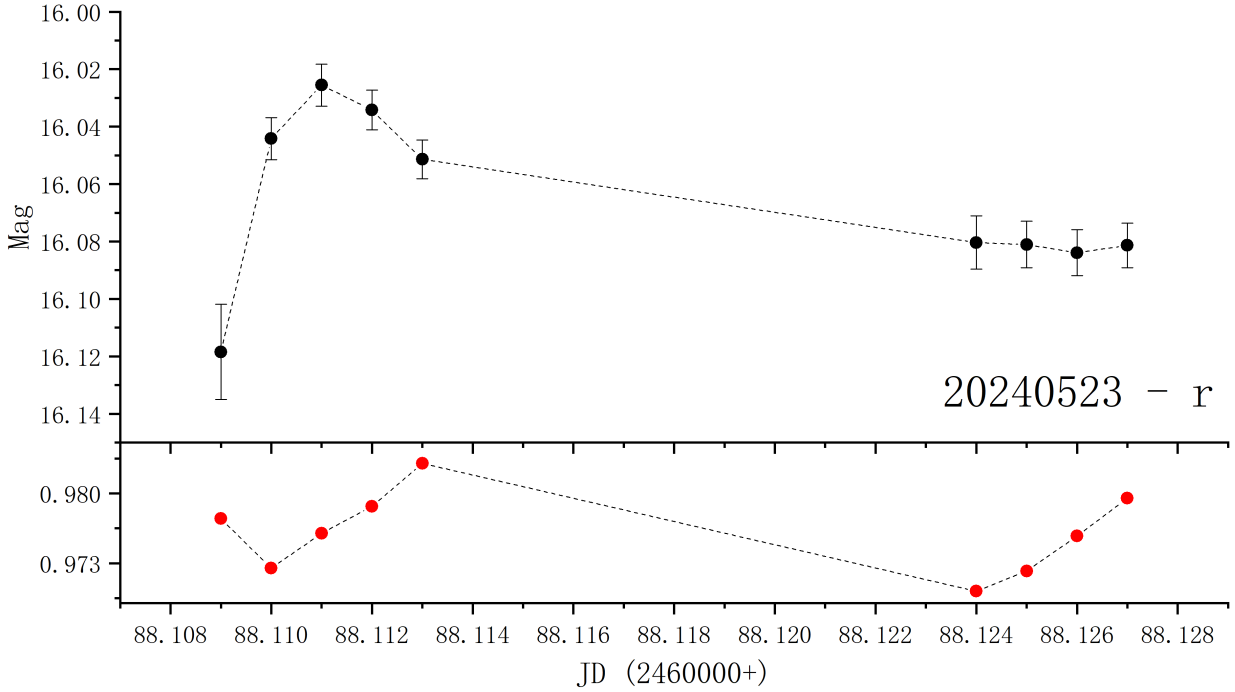
20240523 - r
Mag
16.00
16.02
16.04
16.06
16.08
16.10
16.12
16.14
0.980
0.973
88.108
88.110
88.112
88.114
88.116
88.118
88.120
88.122
88.124
88.126
88.128
JD (2460000+)

v band

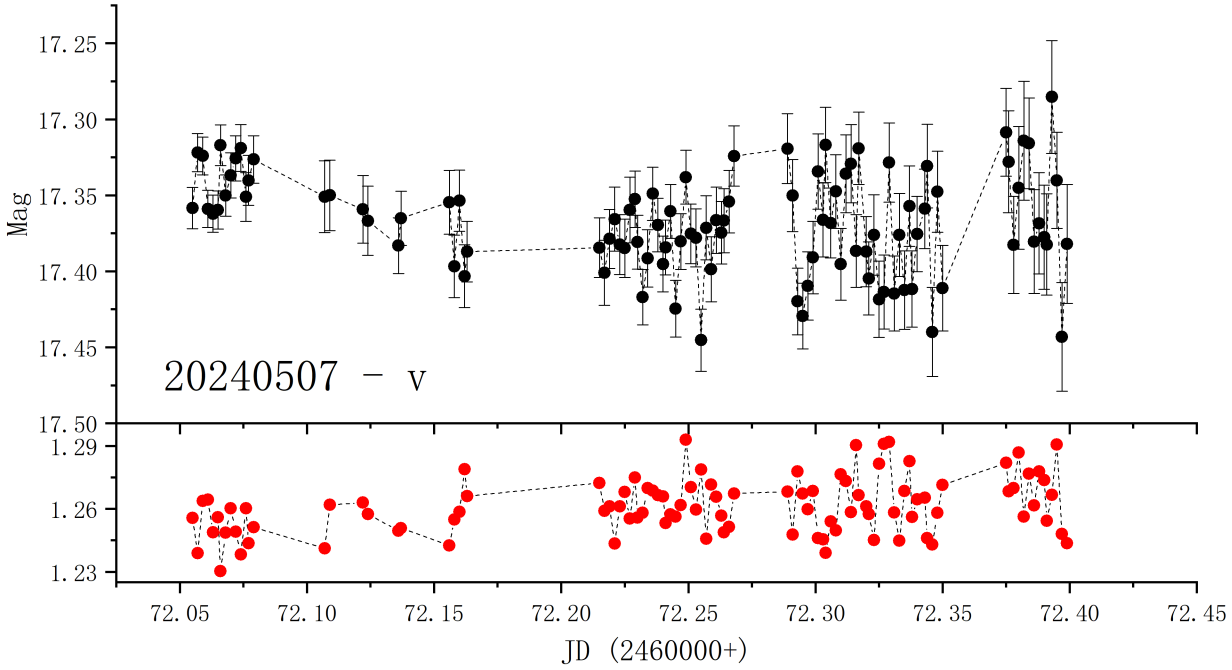
Mag
17.25
17.30
17.35
17.40
17.45
17.50
20240507 - v
1.29
1.26
1.23
72.05
72.10
72.15
72.20
72.25
72.30
72.35
72.40
72.45
JD (2460000+)

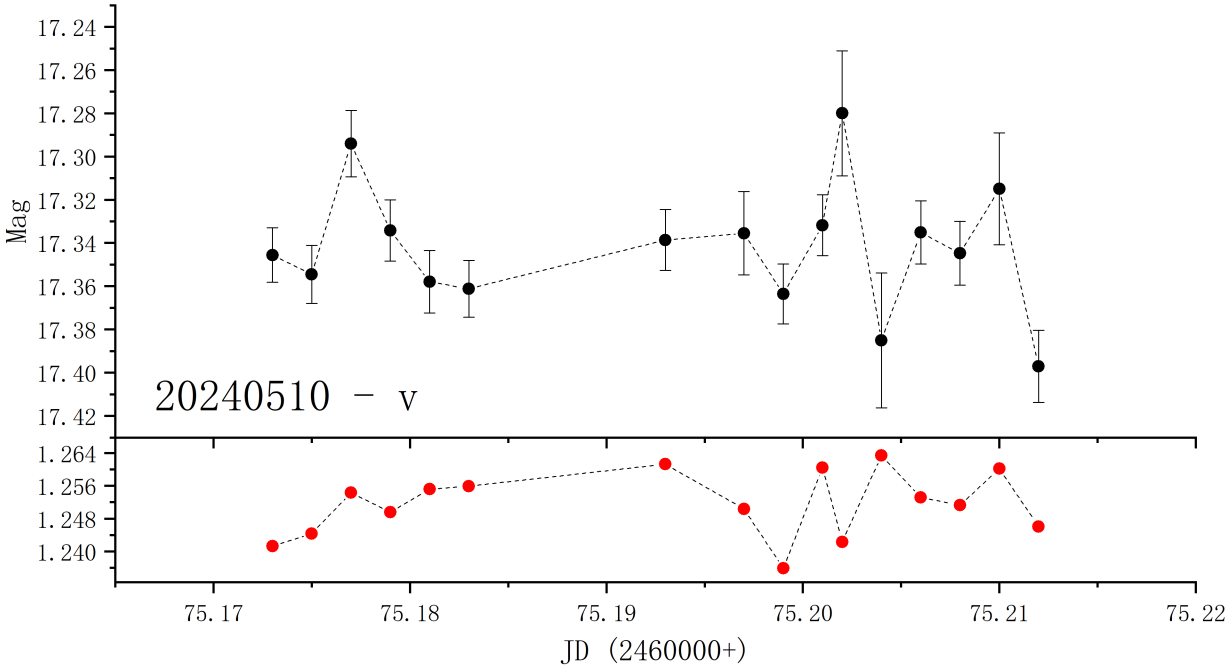
Mag
17.24
17.26
17.28
17.30
17.32
17.34
17.36
17.38
17.40
17.42
20240510 - v
1.264
1.256
1.248
1.240
75.17
75.18
75.19
75.20
75.21
75.22
JD (2460000+)

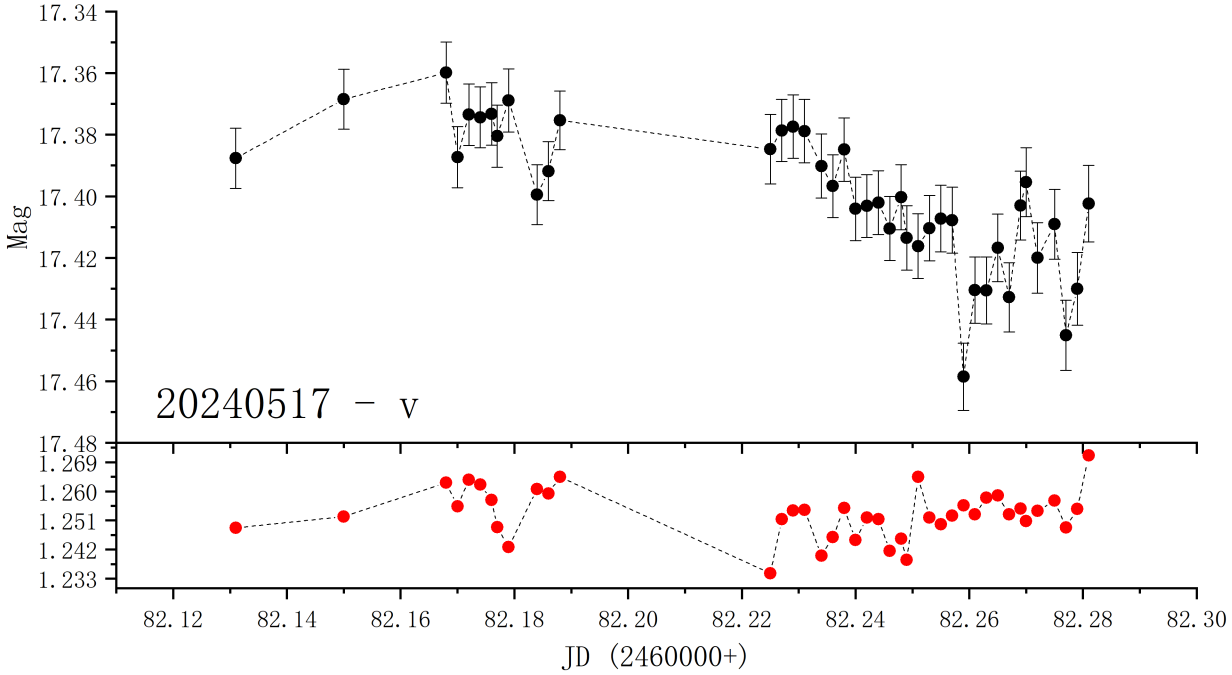
Mag
17.34
17.36
17.38
17.40
17.42
17.44
17.46
17.48
20240517 - v
1.269
1.260
1.251
1.242
1.233
82.12
82.14
82.16
82.18
82.20
82.22
82.24
82.26
82.28
82.30
JD (2460000+)

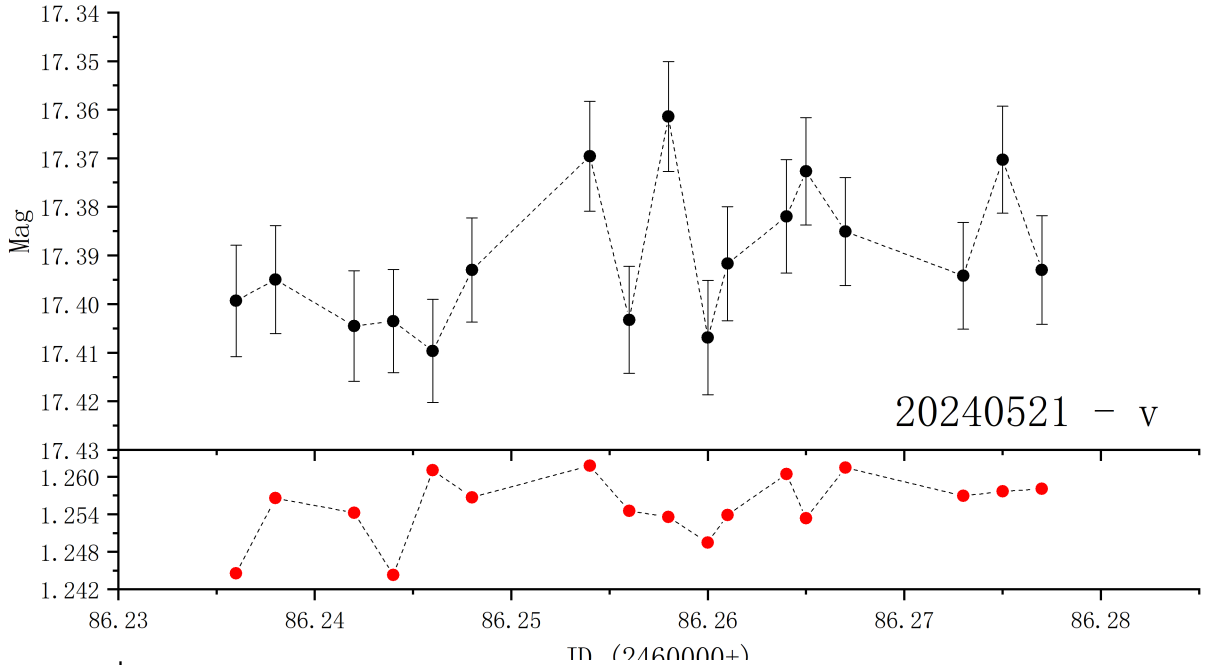
20240521 - v
Mag
17.34
17.35
17.36
17.37
17.38
17.39
17.40
17.41
17.42
17.43
1.260
1.254
1.248
1.242
86.23
86.24
86.25
86.26
86.27
86.28

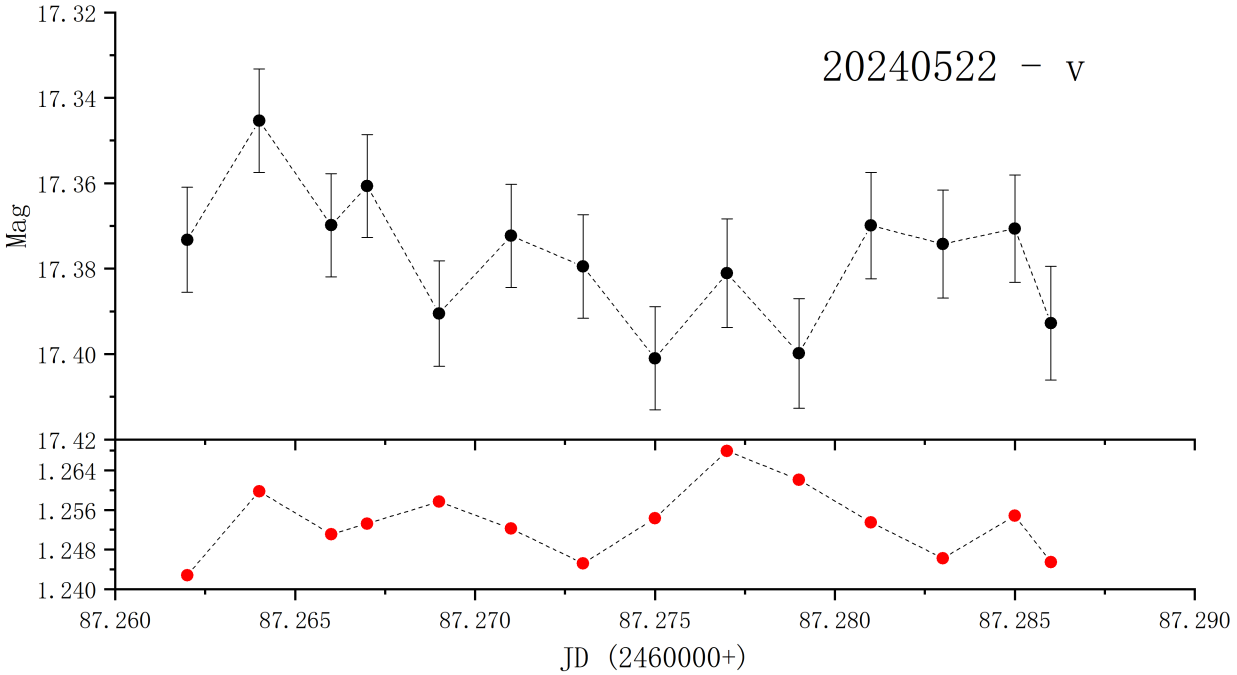
20240522 - v
Mag
17.32
17.34
17.36
17.38
17.40
17.42
1.264
1.256
1.248
1.240
87.260
87.265
87.270
87.275
87.280
87.285
87.290
JD (2460000+)

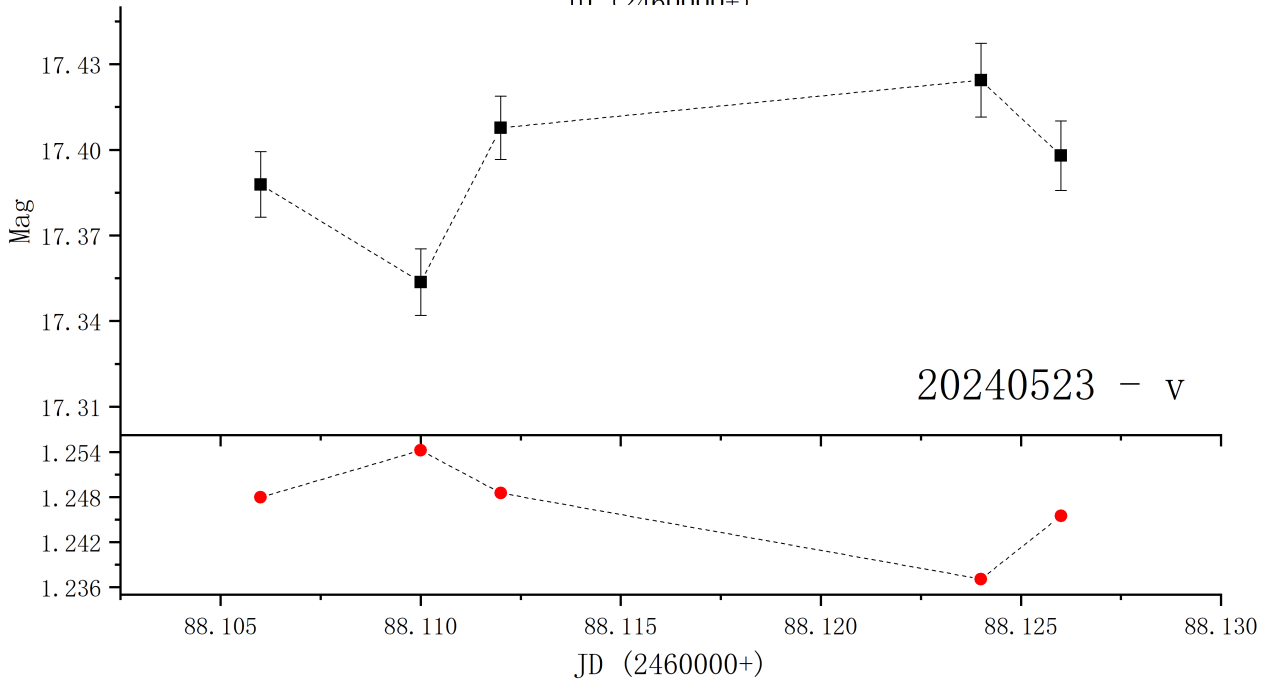
20240523 - v
Mag
17.43
17.40
17.37
17.34
17.31
1.254
1.248
1.242
1.236
88.105
88.110
88.115
88.120
88.125
88.130
JD (2460000+)

	number（g）	均方差（g）	Sextractor平均误差（g）	Amp%（g）
20230429	47	0.00768	0.01588	11.29587
20230502	53	0.00868	0.01887	11.41414
20230503	8	0.01297	0.01510	6.84336
20230506	169	0.00889	0.01816	13.66530
20230508	106	0.00653	0.01493	19.46112
20230511	22	0.00894	0.01430	7.22622
20230518	37	0.00330	0.00810	5.94768
	number（r）	均方差（r）	Sextractor平均误差（r）	Amp%（r）
20230507	171	0.00169	0.00995	10.50527
20230510	23	0.00657	0.00712	5.05527
20230517	66	0.01005	0.00577	6.32927
20230521	34	0.00466	0.00591	6.13275
20230522	27	0.00410	0.00586	5.52260
20230523	9	0.00405	0.00867	9.26635
	number（u）	均方差（u）	Sextractor平均误差（u）	Amp%（u）
20230429	25	0.05036	0.03310	16.94939
20230502	27	0.09206	0.04025	11.46259
20230503	4	0.03191	0.02647	0.79219
20230506	88	0.06043	0.03380	19.31164
20230508	53	0.04202	0.02255	6.86353
20230511	12	0.04020	0.02342	11.82564
20230518	19	0.02215	0.01612	7.74332
	number（v）	均方差（v）	Sextractor平均误差（v）	Amp%（v）
20230507	101	0.02561	0.02272	15.58660
20230510	16	0.02062	0.01727	11.34101
20230517	41	0.01257	0.01052	9.70648
20230521	17	0.01087	0.01117	4.57044
20230522	14	0.01482	0.01240	5.14888
20230523	5	0.01778	0.01187	6.61503

Data Processing Comparison

Data Processing Comparison

- Five days of data with significant changes (2023-04-29, 2023-05-02, 2023-05-08, 2023-05-17, 2023-05-18) were selected to compare the results processed by me with those processed by the lm6 database.
  2.Finally, a comparison of the magnitudes and errors for these five days is provided.

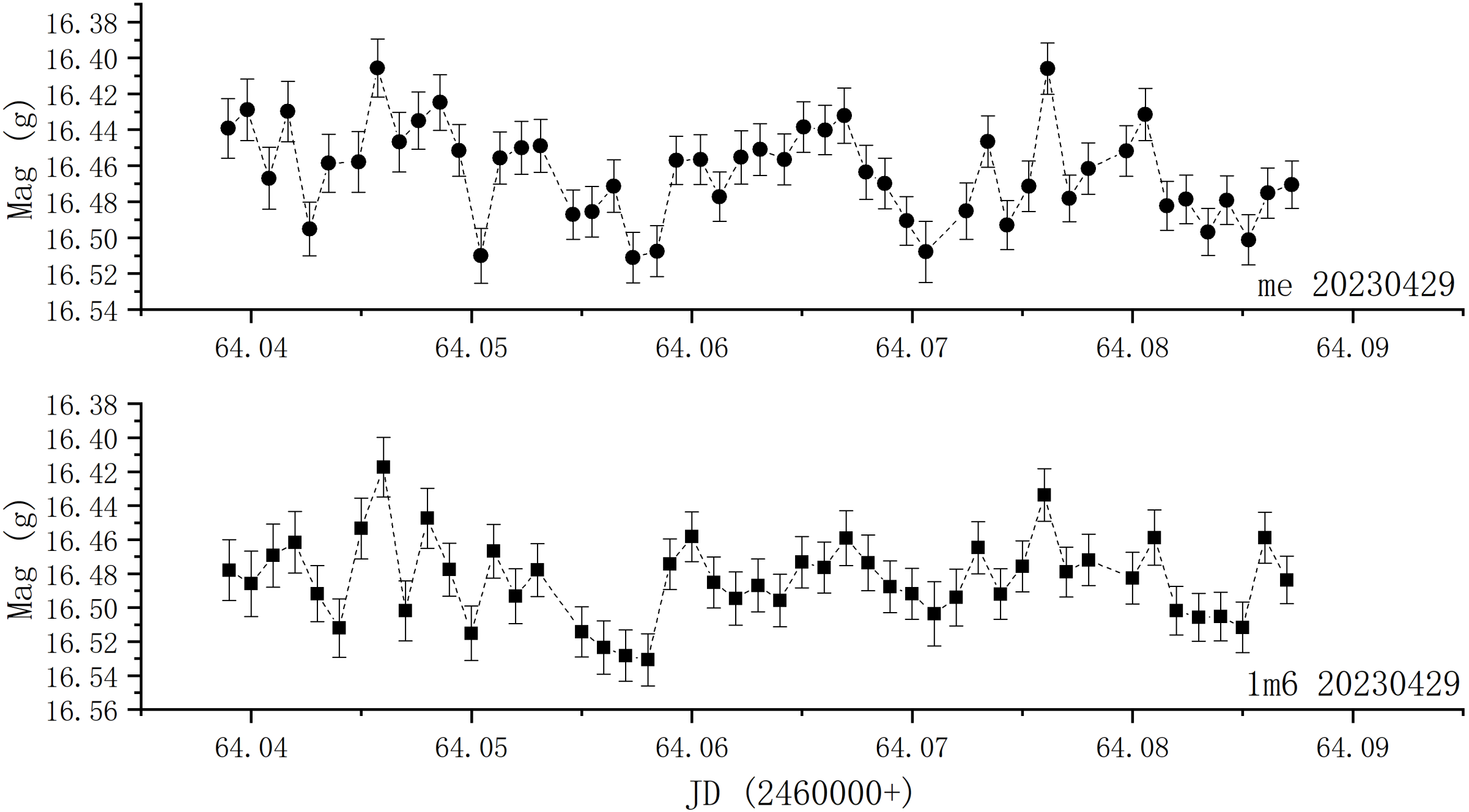
16.38
16.40
16.42
16.44
16.46
16.48
16.50
16.52
16.54
16.56
Mag (g)
64.04
64.05
64.06
64.07
64.08
64.09
me 20230429
1m6 20230429
JD (2460000+)

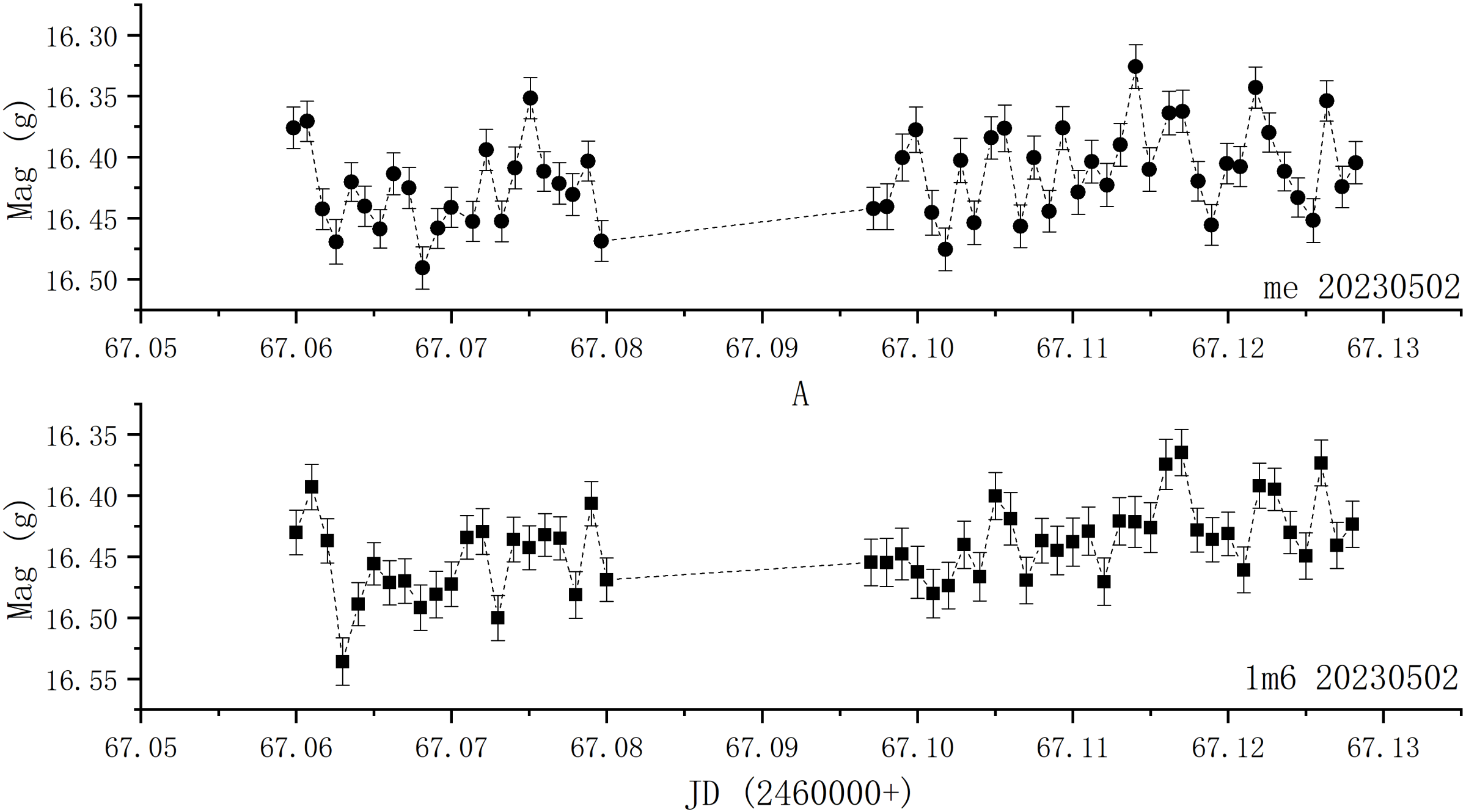
16.30
16.35
16.40
16.45
16.50
Mag (g)
me 20230502
67.05
67.06
67.07
67.08
67.09
67.10
67.11
67.12
67.13
A
16.35
16.40
16.45
16.50
16.55
Mag (g)
1m6 20230502
67.05
67.06
67.07
67.08
67.09
67.10
67.11
67.12
67.13
JD (2460000+)

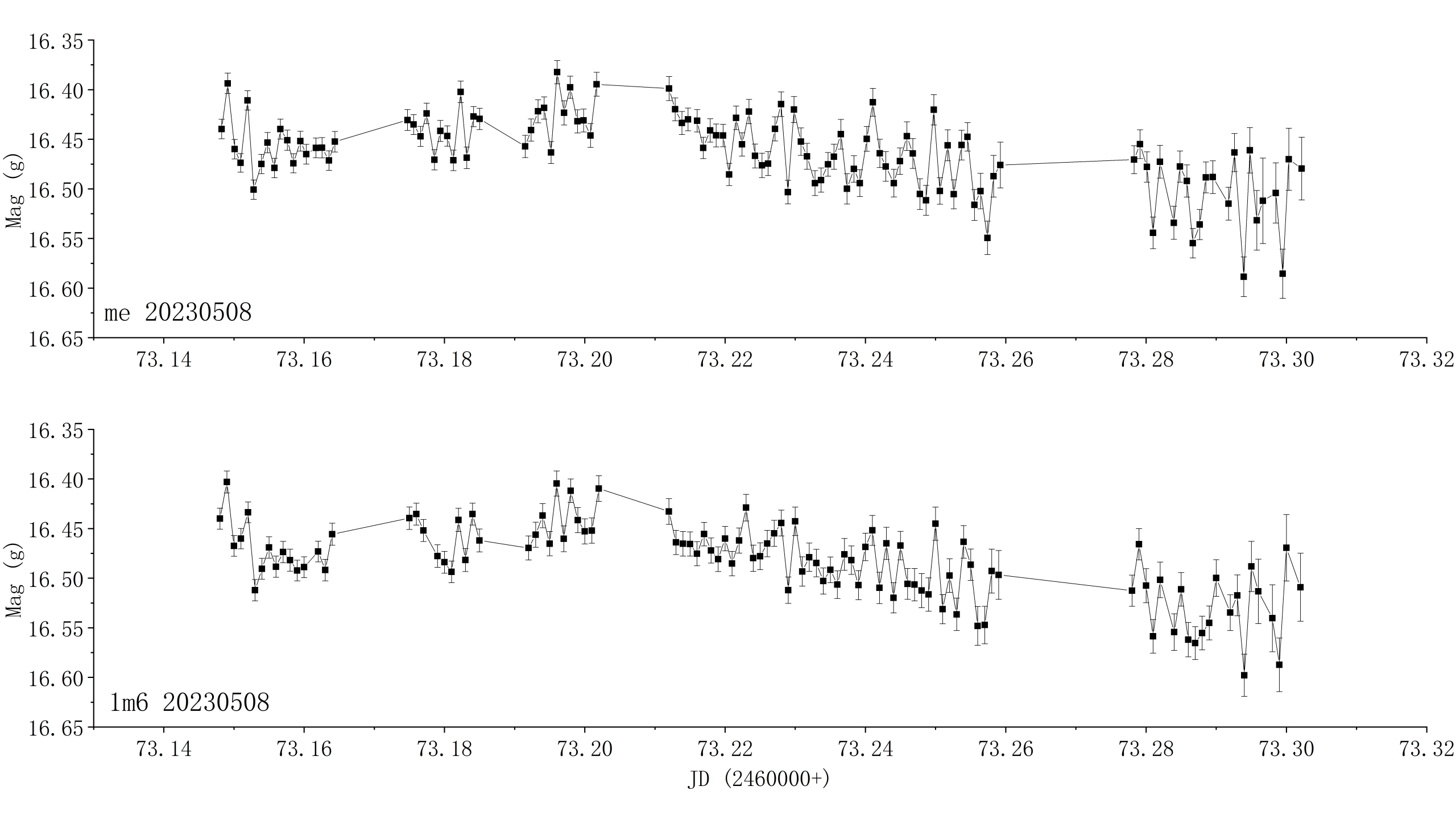
16.35
16.40
16.45
16.50
16.55
16.60
16.65
Mag (g)
me 20230508
73.14
73.16
73.18
73.20
73.22
73.24
73.26
73.28
73.30
73.32
16.35
16.40
16.45
16.50
16.55
16.60
16.65
Mag (g)
1m6 20230508
73.14
73.16
73.18
73.20
73.22
73.24
73.26
73.28
73.30
73.32
JD (2460000+)

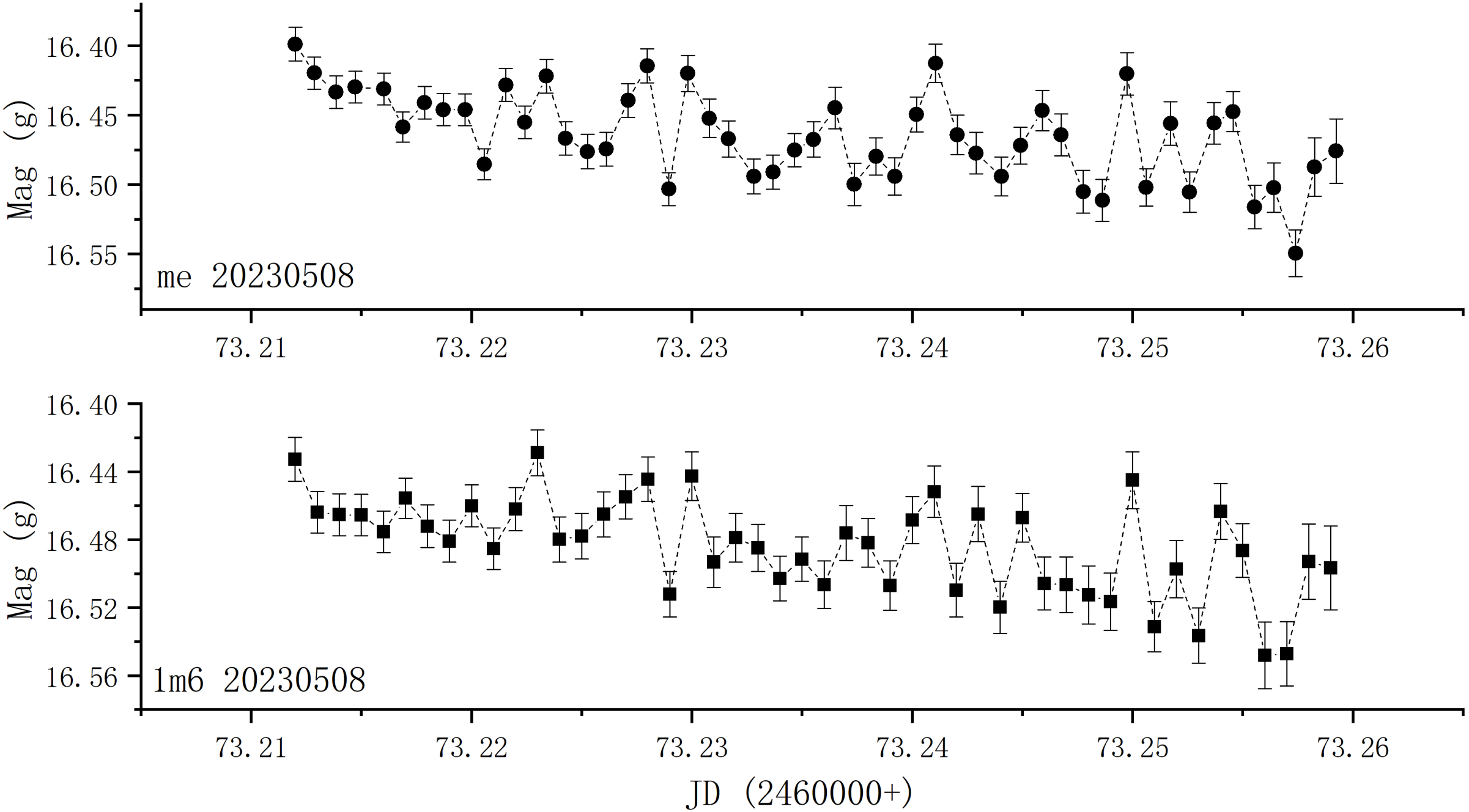
16.40
16.45
16.50
16.55
Mag (g)
me 20230508
73.21
73.22
73.23
73.24
73.25
73.26
16.40
16.44
16.48
16.52
16.56
Mag (g)
1m6 20230508
73.21
73.22
73.23
73.24
73.25
73.26
JD (2460000+)

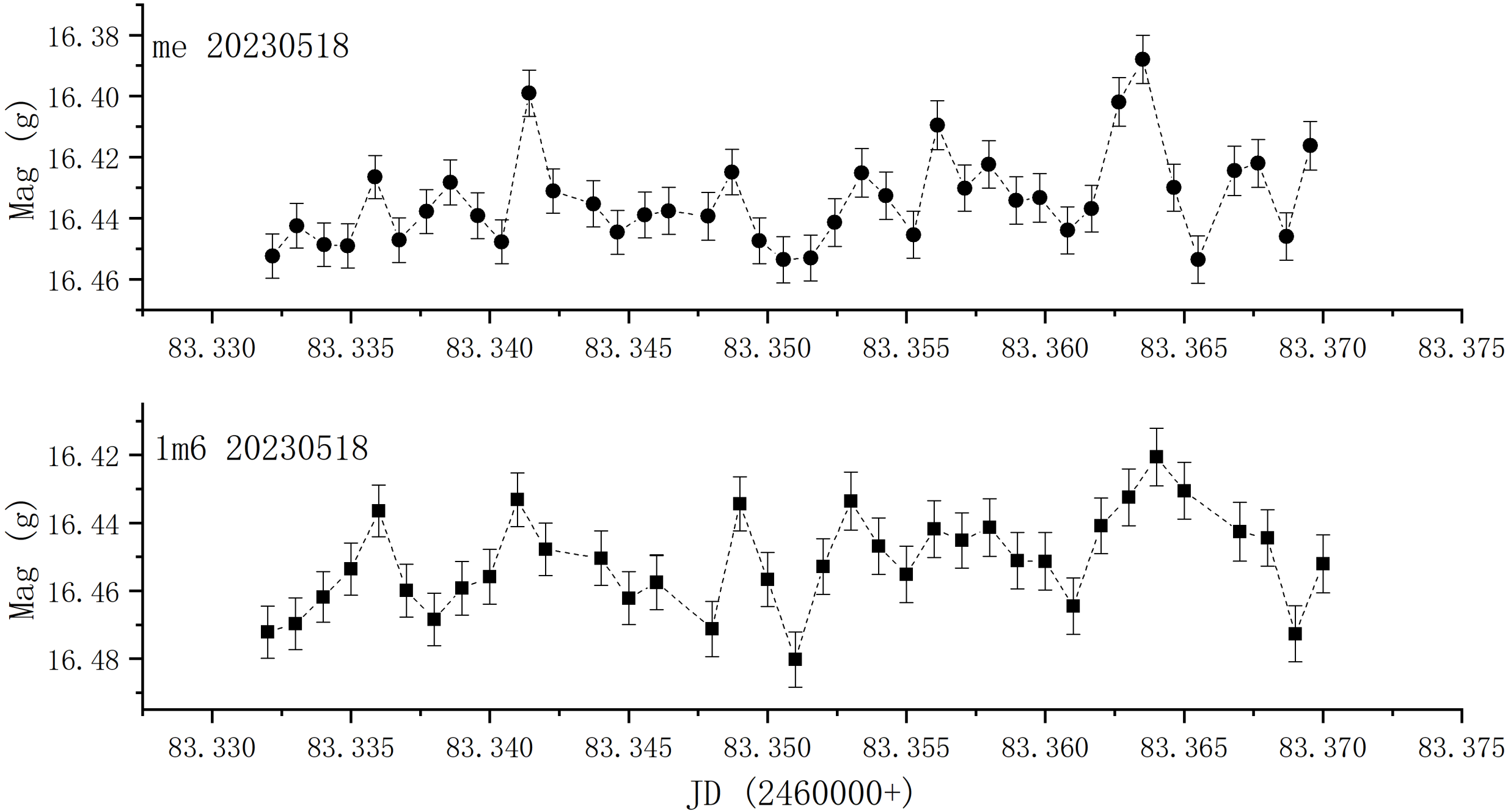
me 20230518
Mag (g)
16.38
16.40
16.42
16.44
16.46
83.330
83.335
83.340
83.345
83.350
83.355
83.360
83.365
83.370
83.375
1m6 20230518
Mag (g)
16.42
16.44
16.46
16.48
83.330
83.335
83.340
83.345
83.350
83.355
83.360
83.365
83.370
83.375
JD (2460000+)

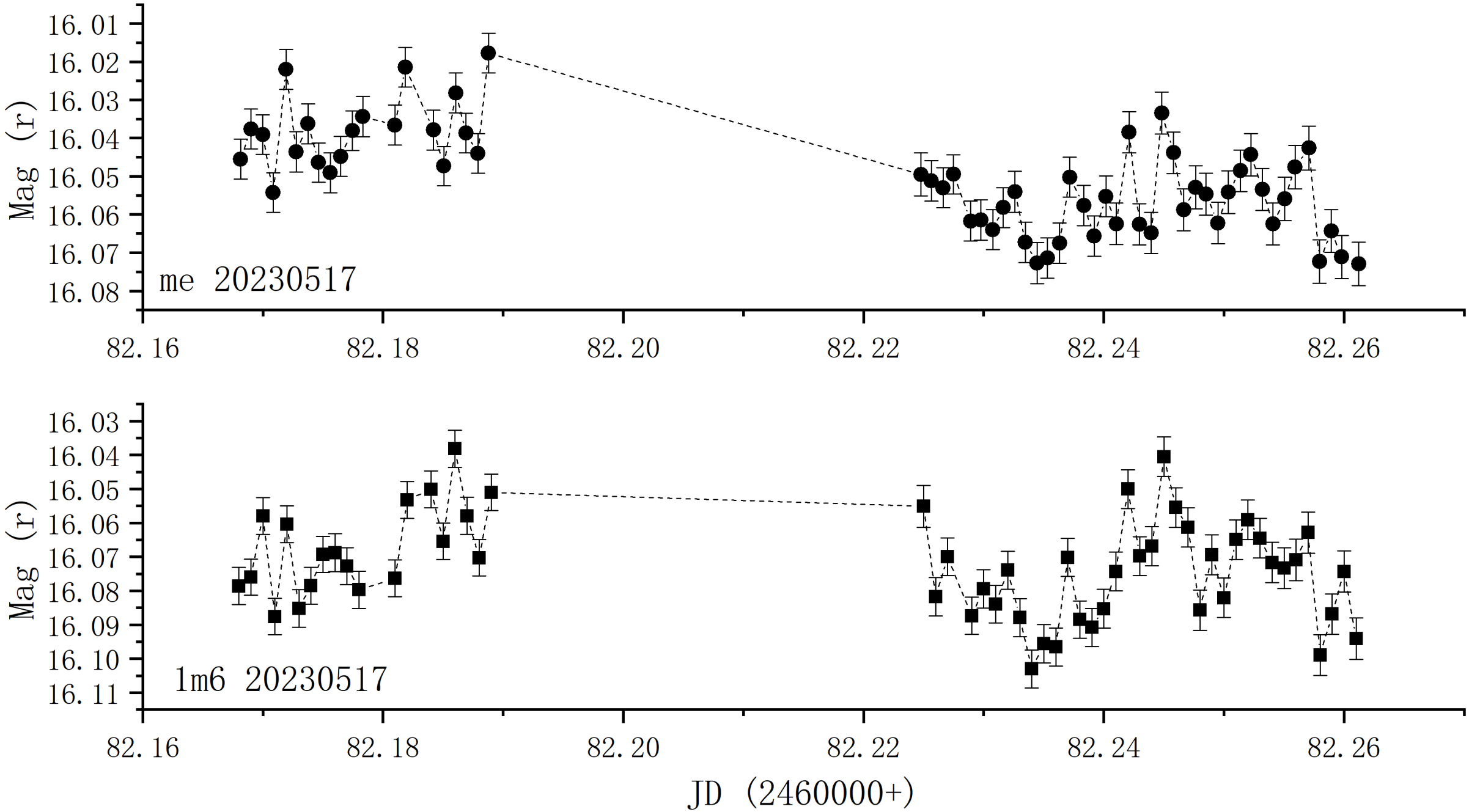
16.01
16.02
16.03
16.04
16.05
16.06
16.07
16.08
Mag (r)
me 20230517
82.16
82.18
82.20
82.22
82.24
82.26
16.03
16.04
16.05
16.06
16.07
16.08
16.09
16.10
16.11
Mag (r)
1m6 20230517
82.16
82.18
82.20
82.22
82.24
82.26
JD (2460000+)

Data Processing Comparison

	平均星等	Sextractor平均误差
me 20230429 (g)	16.46346	0.01468
1m6 20230429 (g)	16.48354	0.01588
me 20230502 (g)	16.41557	0.01714
1m6 20230502 (g)	16.44233	0.01887
me 20230508 (g)	16.46423	0.01387
1m6 20230508 (g)	16.48393	0.01493
me 20230518 (g)	16.43399	0.00759
1m6 20230518 (g)	16.45158	0.00810
me 20230517 (r)	16.05258	0.00550
1m6 20230517 (r)	16.07279	0.00995

- Based on the results, there is a very small difference in the daily average magnitudes between my processing and the processing from the 1m6 database, approximately around 0.02 mag. The difference in the daily average Sextractor errors is also very minimal.

Data Processing Comparison

The root mean square errors (RMS) of the light curves processed by me and those from the 1m6 database for these five days are listed in the table below, with the minimum value being 0.01 and the maximum value being 0.026.

$$\sigma = \sqrt{\frac{\sum_{i=1}^{N}(m_i - \overline{m})^2}{N-1}}$$

	均方差
0429 g	0.017462
0502 g	0.026206
0508 g	0.017238
0517 r	0.010825
0518 g	0.011881

Current outburst of BL Lacertae

The Astronomer's Telegram http://www.astronomerstelegram.org

==========

ATEL #16849 ATEL #16849

Title: Fermi-LAT detection of enhanced gamma-ray activity from the blazar BL Lacertae

Author: P. V. van Zyl (SARAO), G. La Mura (INAF-O. A. Cagliari), Denis Bernard (LLR, Ecole Polytechnique & CNRS / IN2P3), on behalf of the Fermi Large Area Telescope Collaboration
Queries: pfesesani@hartrao.ac.za

Posted: 6 Oct 2024; 23:27 UT
Subjects:Gamma Ray, >GeV, Request for Observations, AGN, Blazar

The Large Area Telescope (LAT), one of the two instruments on the Fermi Gamma-ray Space Telescope, has observed recent increasing gamma-ray activity from BL Lacertae (4FGL J2202.7+4216; The Fermi-LAT collaboration 2020, ApJS, 247, 33), with coordinates R.A. = 330.68038 deg, Decl. = +42.27778 deg (J2000; Johnston et al. 1995, AJ, 110, 880), and redshift z = 0.0686 (Vermeulen et al. 1995, ApJ, 452, L5).

Preliminary analysis indicates that this source was in an elevated gamma-ray emission state on 2024 October 5, with a daily averaged gamma-ray flux (E>100MeV) of (10.4+/-0.5) x 10^-6 photons cm^-2 s^-1 (statistical uncertainty only), corresponding to a flux increase of a factor of about 20 relative to the average flux reported in the fourth Fermi-LAT catalog (4FGL-DR4). The photon index is 1.9 +/- 0.1, corresponding to a significantly harder spectrum than the 4FGL catalog value of 2.13 +/- 0.01. The spectral hardening resulted in the detection of nine high-energy (E > 10 GeV) photons, having probability to be associated with the source larger than p = 0.999, the highest energy of which was close to 180 GeV. We have previously reported enhanced activity from this source in ATels #15688, #14330 and #14072.

Because Fermi normally operates in an all-sky scanning mode, regular gamma-ray monitoring of this source will continue. Preliminary light curves for BL Lacertae can be accessed via the Fermi-LAT Monitored Source List at https://fermi.gsfc.nasa.gov/ssc/data/access/lat/msl_lc/source/BL_Lac; and via the Fermi-LAT Light-Curve Repository at https://fermi.gsfc.nasa.gov/ssc/data/access/lat/lcr/source.html?source_name=4FGL_J2202.7+4216.
We encourage multifrequency observations of this source. For this source, the Fermi-LAT contact person is Simone Garrappa (simone.garrappa at desy.de).

The Fermi-LAT is a pair conversion telescope designed to cover the energy band from 20 MeV to greater than 300 GeV. It is the product of an international collaboration between NASA and DOE in the U.S. and many scientific institutions across France, Italy, Japan and Sweden.

Current outburst of BL Lacertae

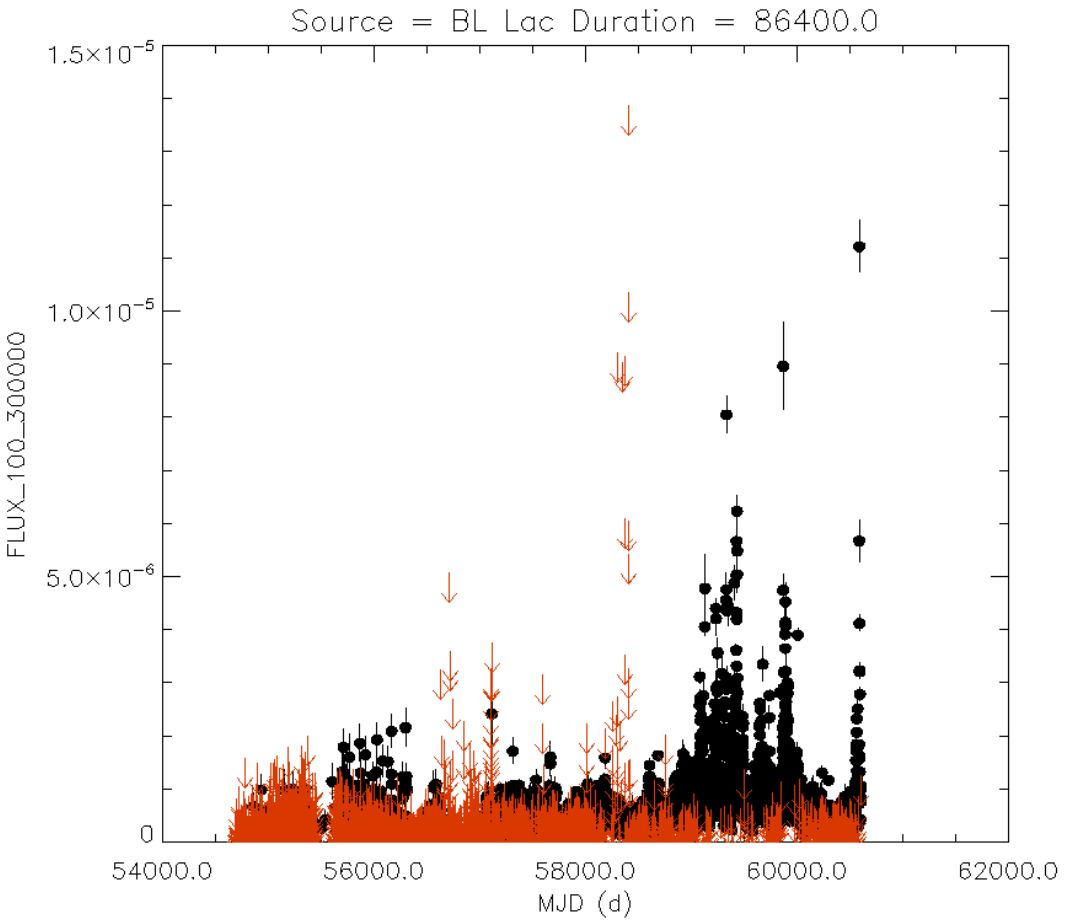

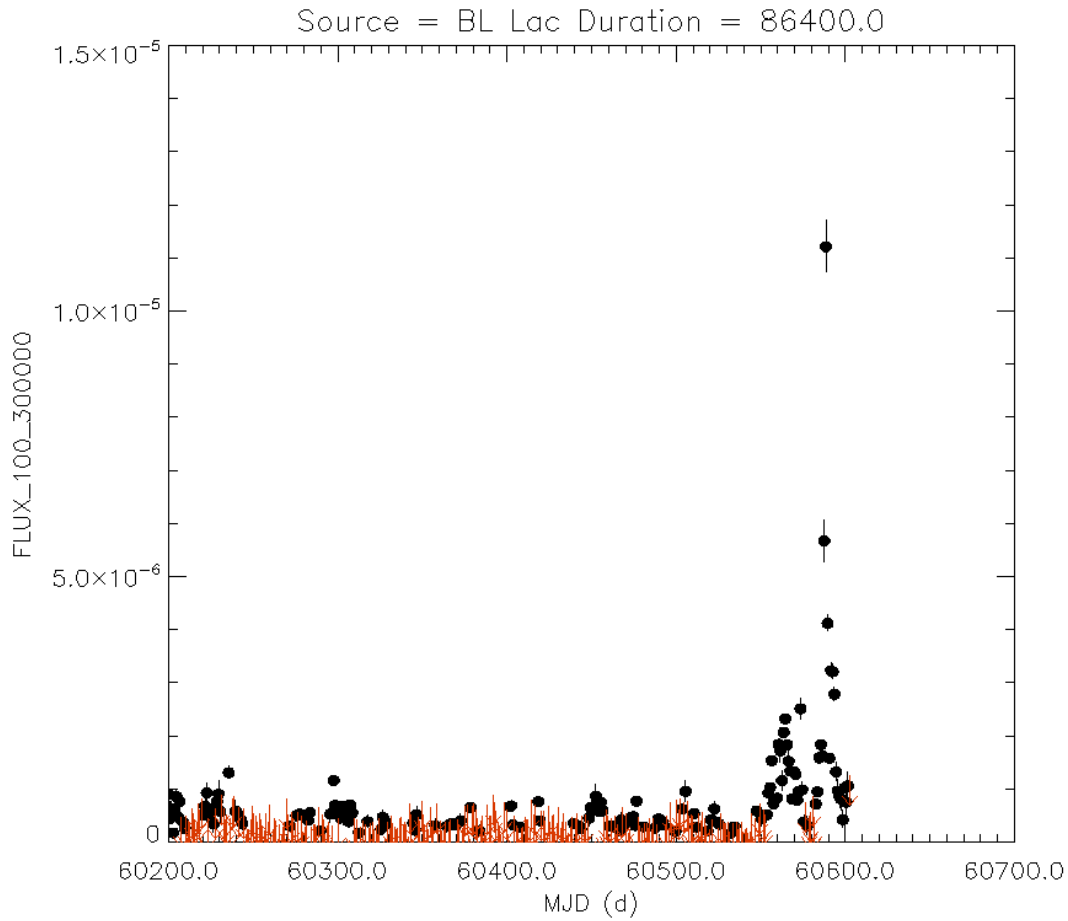

Current outburst of BL Lacertae

- Preliminary analysis indicates that this source was in an elevated gamma-ray emission state on 2024 October 5, with a daily averaged gamma-ray flux (statistical uncertainty only), corresponding to a flux increase of a factor of about 20 relative to the average flux reported in the fourth Fermi-LAT catalog (4FGL-DR4).
- Utilizing the LHAASO-WCDA real-time alert system, here we report the detection of a TeV gamma-ray flare from AGN BL Lacertae. LHAASO-WCDA observed a gamma-ray flux enhancement from the active galactic nuclei BL Lacertae, commencingat MJD 60588.43.
- The VERITAS (Very Energetic Radiation Imaging Telescope Array System) detection of very-high-energy (VHE; E> 100 GeV) flaringactivity in BL Lacertae.
- The Large Array Survey Telescope (LAST)

Current outburst of BL Lacertae

- Swift observations (ID 21169, 21248), which were performedon Sep 24, 25, 26, and Oct 5, 6, 7, 2024.
- Date, V, B, U,

  Sep 24, 14.18 (+/-0.05), 15.07 (+/-0.04), 14.79 (+/-0.05),

  Sep 25, 13.84 (+/-0.04), 14.59 (+/-0.03), 14.19 (+/-0.04), 14.87 (+/-0.05),

  Sep 26, 14.42 (+/-0.04), 15.27 (+/-0.04),

  Oct 5, 12.80 (+/-0.03), 13.55 (+/-0.03), 13.04 (+/-0.03),

  Oct 6, 13.79 (+/-0.03), 14.54 (+/-0.03), 14.08 (+/-0.03),

  Oct 7, 13.87 (+/-0.03), 14.71 (+/-0.03), 14.26 (+/-0.03).

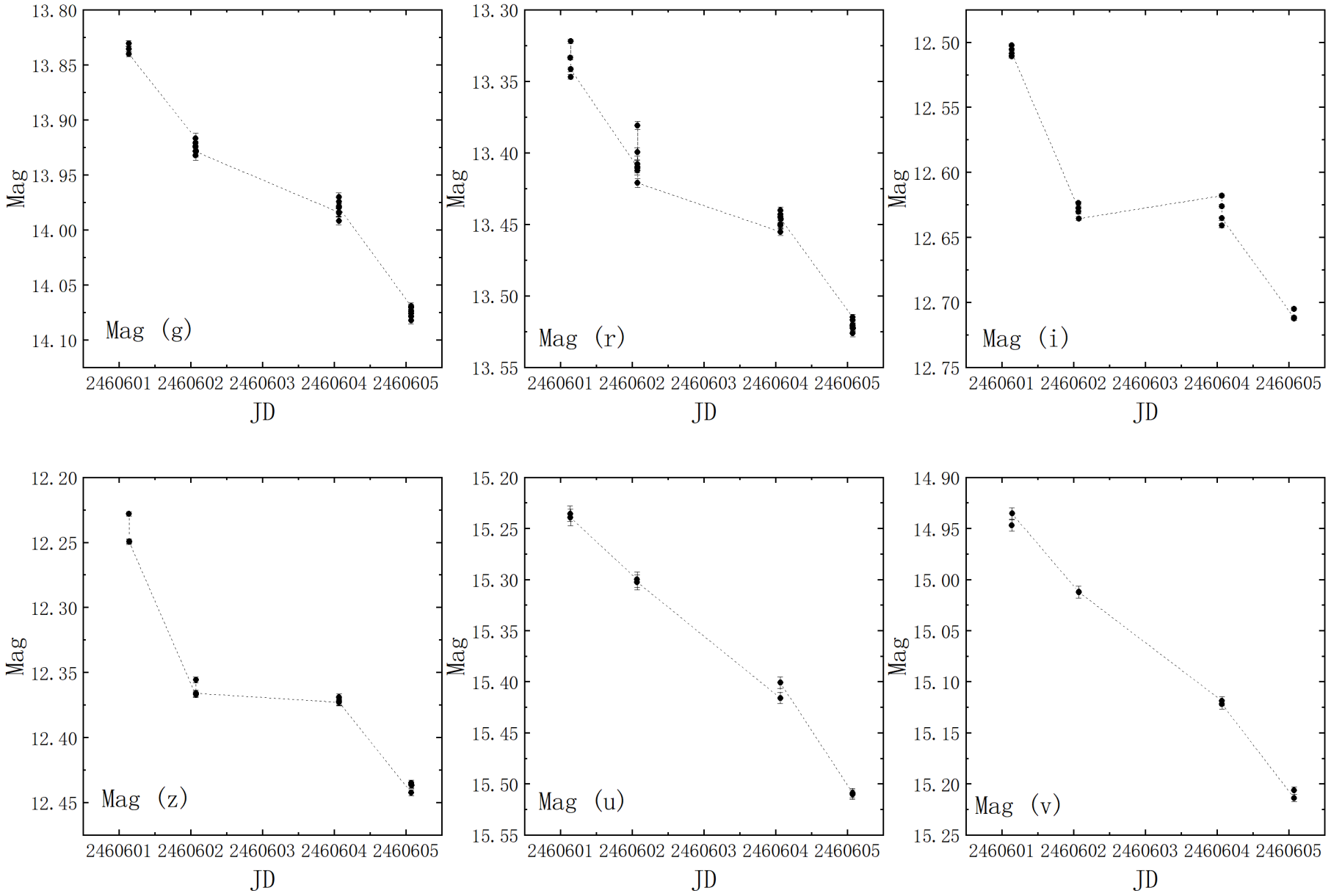

- BL Lacertae observations of 1m6 on October 17, 18, 20, and 21

Current outburst of BL Lacertae

- Based on a large number of detectors, the full-band spectrum covering from radio to gamma-ray bands can be obtained. The SED spectrum in logarithmic space allows for an intuitive observation of the spectral properties across various bands, thereby facilitating the analysis of related physical mechanisms.
- The energy spectrum of blazars features two peaks: the low-energy peak spanning from radio to ultraviolet bands, and the high-energy peak ranging from X-rays to high-energy gamma rays.
- The spectral energy distribution (SED) of blazars is divided into two parts: The first part peaks in the radio to X-ray bands, possibly explained by synchrotron radiation from relativistic electrons; the second part peaks in the X-ray to gamma-ray bands, mainly attributed to inverse Compton scattering of low-energy photons by extremely relativistic electrons.